Politecnico di Torino

M. Sc. Environmental and Land Engineering – Climate Change

A.a. 2023/2024

Graduation Session December 2024

Numerical Modelling of Cement Grout Degradation in a Single Rock Fracture

Supervisors:

    Prof. Rajandrea Sethi

    Prof. Liangchao Zou

Candidate:

    Francesco Tisselli

Abstract

The construction of infrastructures such as dams requires a stable ground for the foundations to lay on, which also have to be protected from erosion deriving from groundwater exposure. One way to achieve this is to grout the rock fractures present in the bedrock using cement. However, the continuous flow of groundwater will, over time, cause the deterioration of the grout by dissolving and mobilising the mineral phases resulting from the hydration process. This study aims to determine the variations in porosity and hydraulic conductivity induced by the dissolution of portlandite present in the grout under the influence of groundwater flow. Two different cases have been simulated in COMSOL Multiphysics®, one being a two-dimensional fracture with infinite extent, while the other is a three-dimensional geometry. Each model has two main components, one for the flow simulation and one for the transport. The COMSOL Multiphysics® modules used in this study are Darcy's Law and Transport of Diluted Species in Porous Media. The software PHREEQC was used to determine the chemical species concentration for both the initial and boundary conditions. The results show that, at the end of 20 years, the mineral concentration decreases from the initial molarity of 1035.98 mol/m^3 to values lower than 20 mol/m^3, with the 2D model reporting the strongest variation. The pH values dropped from 12.951 to 8.65 or less. This leads to an increase in porosity by 3.45%, while hydraulic conductivity increases by 9.64%.

Keywords: groundwater; modelling; portlandite; transport; grouting; COMSOL Multiphysics.

Table of Contents

List of Figures

List of Tables

1   Introduction

Groundwater systems are complex formations, influenced by different elements such as geology, topography, climate, and vegetation. Hydrogeology and groundwater engineering, the branches of science that study aquifers, pay close attention to the groundwater flow and the latter's interactions with the surrounding geology. These interactions cause the underground water to contain different amounts of dissolved chemical species, depending on the type of rocks present in the system and other physical properties. In some cases, it is necessary to forecast how an aquifer will behave over time from both a flow and chemical point of view, and in such instances, groundwater models represent a valid and reliable option. Out of all the kinds of models available, numerical ones can be used for problems in which the variables that describe the domain assume values that vary in space and time. Even though numerical models can solve complex algebraic equations referred to a specific case, they will always be a simplistic representation of the considered reality (Fetter and Kreamer, 2022).

When constructing infrastructures such as dams, it is of critical importance to investigate the conditions of geological formations underlying the structure. If the ground supporting the dam is a heterogeneous rock mass, meaning that it's composed of blocks of rock and discontinuities such as fractures, the risk of structural failures can increase (Fernandez-Gutierrez *et al.*, 2021). An effective approach to offset the lack of adequate mechanical properties in heterogenous rock masses is using grouting reinforcement technology. By

introducing cement grout into the fractures, their strength and deformation will increase, depending on the rheological properties of the injected substance, therefore inducing an overall enhancement in the mechanical properties of the rock mass itself. Moreover, the low permeability associated with grouting materials reduces the overall groundwater flow in the area, preventing the subsurface fluid from reaching the dam foundations and defending them from erosion and chemical degradation (Liu *et al.*, 2018). Different types of grouting materials could be used during the process, among them the Portland cement-based ones have gained interest over the years, because of their low price, moderate environmental impacts, and good performance through time (Sha *et al.*, 2019). The purpose of this analysis is to study how the cement grout infilled in a single rock fracture present in the bedrock, which is injected to prevent the dam foundation erasure and improve the mechanical properties of the geology, hydraulic properties and mineralogic composition will change because of the groundwater flow.

Despite its good performance, ordinary Portland cement (OPC) based grout can undergo degradation due to groundwater flow through the solid matrix. Depending on the groundwater's chemical composition, the phases that make up the OPC grout will dissolve, and the resulting aqueous species will be carried away, causing variations in the hydraulic properties of the concrete (Luna, Arcos and Duro, 2006). The expected results of these groundwater-grout interactions are an increase in porosity and hydraulic conductivity of the solid matrix, which will in turn affect the flow behavior leading to an iterative procedure. Since the subsurface water movement and the geochemical degradation are so tightly correlated, it is of key importance to create a model in which they are coupled so that the results will have higher accuracy as opposed to the ones obtained from a disjunct analysis (Idiart and Shafei, 2019). Predicting the cement grout performance correctly allows a more precise design of the infrastructure, lowering the risks of structural instabilities and failures.

1.1 Aim and Objectives

While previous literature focuses on the degradation of cement vaults used to contain radioactive and toxic waste, this master's thesis aims to assess the changes in porosity

1 – INTRODUCTION

and hydraulic conductivity, through the use of the software COMSOL Multiphysics®, of the cement grout utilized to seal a single rock fracture underlying a dam, following groundwater flow-induced degradation. The results of this analysis could be integrated into future research focused on the evaluation of structural instabilities in the interested dam. The study will be carried out through the following objectives:

- Construct a groundwater flow model of both a two-dimesional and three-dimensional rough fracture filled with cement grout, considered as a porous material, in COMSOL Multiphysics®.
- Analyze the variation in concentration of the mineral and other three species over 20 years, as well as assess how the pH of the domain changes in time.
- Determine the changes in porosity and hydraulic conductivity caused by the previous results.

2 Theoretical Background

2.1 Groundwater Flow

Groundwater reservoirs are subsurface entities composed of a porous medium and water. The former is characterized by the ability to store water within itself as well as to allow its flow, depending on the values of different aquifer properties (Sethi and Di Molfetta, 2019).

2.1.1 Porosity

As diagenetic processes form rocks, the loose sediments are rearranged in such a way that they aren't in complete contact with each other but are separated by void spaces. The number of voids present in the rock is influenced by various factors like the spatial disposition of the sediment grains, their shape and size distribution, compaction caused by the weight of successive deposition of materials, precipitation and dissolution of mineral phases. As a result, the volume of voids of the final rock formation will typically be lower than the initial one. Porosity is a term used to indicate the fraction of a rock that isn't composed of a solid matrix and that is therefore capable of hosting fluids. Consequently, it can be defined as

$$n = \frac{V_v}{V_T} \tag{1}$$

Where:

n is the porosity (-)

V_v is the volume of voids (L^3)

V_T is the total volume of the rock (L^3)

It must be noted that not all pores can contain nor allow the flow of water, as some of them together with the pore throats, could be smaller than the water molecules themselves and some others may not be interconnected at all. Because of this, it is reasonable to define a new property, the effective porosity (n_e), as the portion of void spaces that are available for groundwater flow (Fetter and Kreamer, 2022). Values assumed by porosity can vary between 0 to 0.48 (Sethi and Di Molfetta, 2019).

2.1.2 Darcy's Law

Groundwater movement is governed by the different kinds of energy stored within itself in mechanical, thermal, and chemical form. In particular, the mechanical component can be represented through the concept of hydraulic head, which is the sum of kinetic, potential, and pressure energies per unit of weight

$$h = \frac{v^2}{2g} + z + \frac{P}{\rho g} \tag{2}$$

Where:

v is groundwater velocity (LT^{-1})

z is the elevation of the groundwater center of mass (L)

P is the pressure ($ML^{-1}T^{-2}$)

Keeping in mind that groundwater tends to move extremely slowly, equation (8) can be rewritten neglecting the kinetic energy term

$$h = z + \frac{P}{\rho g} = z + h_P \qquad (3)$$

Where:

h_P is the pressure head (L)

As the fluid moves through the small pores in the porous medium, frictional forces dissipate part of the hydraulic head, therefore converting mechanical energy into thermal. It can be concluded that groundwater flows from regions with high hydraulic heads to ones with lower values.

Darcy's Law is a linear equation that describes groundwater flow by relating the discharge flowing across a section of porous medium to the variation of hydraulic head over the path considered

$$Q = -KA\frac{dh}{dl} = -KAi \qquad (4)$$

Where:

Q is the water discharge (L^3T^{-1})

A is the cross-sectional area of the medium (L^2)

dl is the length of the path that groundwater follows (L)

K is the hydraulic conductivity (LT^{-1})

i is the hydraulic gradient (-)

It's possible to obtain a velocity from equation (10) by dividing both members by the cross-sectional area, and the resultant parameter is known as Darcy flux or specific discharge. The latter is not the velocity that the fluid experiences as it moves in the aquifer, since groundwater can only flow through the interconnected pores. Darcy flux is an apparent velocity that corresponds to the one that the fluid would have if it was flowing in an open channel. The effective velocity, named seepage velocity of average linear velocity, has to consider only the fraction of the area available for flow, and its formula is (Fetter and Kreamer, 2022)

$$v_x = -\frac{K}{n_e} i \tag{5}$$

Where:

v_x is the average linear velocity (LT^{-1})

The equations (10) and (11) can be used to describe groundwater flow in isotropic aquifers, where the value of hydraulic conductivity is constant across all directions. However, when the properties of the porous medium vary spatially, Darcy's law is redefined in tensorial form

$$\boldsymbol{q} = -\boldsymbol{K}\nabla h \tag{6}$$

If the hydraulic conductivity tensor has been reduced in its identity tensor form by choosing the appropriate reference system, the Darcy flux components are defined as (Sethi and Di Molfetta, 2019)

$$q_{xx} = -K_{xx}\frac{\partial h}{\partial x} \tag{7}$$

$$q_{yy} = -K_{yy}\frac{\partial h}{\partial y} \tag{8}$$

$$q_{zz} = -K_{zz}\frac{\partial h}{\partial z} \tag{9}$$

2.1.2.1 Validity of Darcy's Law

Darcy's law is a simple empirical expression that can be applied in many cases, but some conditions must be respected for it to be used. First, the flow domain has to be in steady state, meaning that the flow conditions won't change over time, or that the changes are negligible. Secondly, the flow must be single phase, so the aquifer has to be saturated in groundwater and air can't be present (Sethi and Di Molfetta, 2019). Thirdly, the fluid

velocity is sufficiently slow to allow the flow regime to be laminar. The flow regime can be determined by using the Reynolds number

$$Re = \frac{\rho g d}{\mu} \qquad (10)$$

Where:

Re is the Reynolds number (-)

d is the grain diameter (L)

For the flow to be laminar Reynolds number must range from 1 to 10, in most cases groundwater flows slowly enough for the condition to be satisfied, while if higher the flow regime is said to be turbulent (Fetter and Kreamer, 2022).

2.1.3 Hydraulic Conductivity

As seen in Equation (4) hydraulic conductivity is the discharge that, under a unitary hydraulic gradient, passes through a unit cross-sectional area of medium. Usual values of K span from 10^{-1} m/s to 10^{-6} m/s but depending on the case they can also go from 10 m/s to 10^{-9} m/s (Sethi and Di Molfetta, 2019).

Hydraulic conductivity is a function of both the fluid and the porous medium, to prove this another property called intrinsic permeability, or more simply permeability, which depends only on the solid matrix has to be considered. The following relationship interconnects the two coefficients

$$K = \frac{\rho g k}{\mu} \qquad (11)$$

Where:

ρ is the fluid density (ML^{-3})

g is the acceleration of gravity (LT^{-2})

k is the intrinsic permeability (L^2)

μ is the dynamic viscosity of the fluid $(ML^{-1}T^{-1})$

Equation (3) shows that K depends on the fluid density and dynamic viscosity, which in turn both depend on the fluid temperature and its ionic composition. This implies that, albeit the permeability remains constant, a change in the last two properties will induce variations in hydraulic conductivity (Fetter and Kreamer, 2022).

Aquifers are formed under many different environmental pressures, resulting in complex anisotropic geologic formations. Given its dependency on the solid matrix, hydraulic conductivity varies based on the direction considered, with the horizontal values usually being higher than the vertical ones (Sethi and Di Molfetta, 2019). Part of the reason behind this difference is the downward stress exerted by both the groundwater and the matrix masses, known as total stress. The latter can be broken down into two components: a compressing one arising from the matrix, called effective stress, and an opposite tensile one related to the fluid pressure. The total stress can therefore be expressed as

$$\sigma_T = \sigma_e + P \tag{12}$$

Where:

σ_T is the total stress $(ML^{-1}T^{-2})$

σ_e is the effective stress $(ML^{-1}T^{-2})$

P is the upward fluid pressure $(ML^{-1}T^{-2})$

A change in total stress value will also induce changes in the two subcomponents (Fetter and Kreamer, 2022). This implies that the hydraulic conductivity can be written in tensorial form

$$\mathbf{K} = \begin{pmatrix} K_{xx} & K_{xy} & K_{xz} \\ K_{yx} & K_{yy} & K_{yz} \\ K_{zx} & K_{zy} & K_{zz} \end{pmatrix} \tag{13}$$

Considering the off-diagonal elements in matrix (5), the following relationships are true: $K_{yx} = K_{xy}$, $K_{zx} = K_{xz}$, and $K_{zy} = K_{yz}$. If, when choosing a reference system, one of the

reference axes is said to correspond to the direction of maximum permeability, then (13) can be reduced to an identity tensor:

$$\boldsymbol{K} = \begin{pmatrix} K_{xx} & 0 & 0 \\ 0 & K_{yy} & 0 \\ 0 & 0 & K_{zz} \end{pmatrix} \tag{14}$$

When the three diagonal components are different from one another, that is for most of the cases, the aquifer is anisotropic. If instead, they assume similar values the following approximation is then valid

$$K_{xx} = K_{yy} = K_{zz} = K \tag{15}$$

and in such cases, the groundwater reservoir is said to be isotropic (Sethi and Di Molfetta, 2019).

2.1.4 Mass Transport

So far, only the movement of groundwater has been discussed. However, subsurface waters always carry with them a certain quantity of dissolved solids and gases, hence their composition is different from the one of pure water. As groundwater flows, these solutes will move as well due to three main transport mechanisms: molecular diffusion, advection, and mechanical dispersion (Fetter and Kreamer, 2022).

2.1.4.1 Molecular Diffusion

Molecular diffusion is a transport mechanism that moves solutes from high-concentration areas to low-concentration areas due to Brownian motes (Fetter and Kreamer 2022). In steady-state conditions, a chemical specie flux in a medium can be described using Flick's law of diffusion (Sethi and Di Molfetta, 2019)

$$j_{M,x_i} = -D_d \frac{\partial C}{\partial x_i} \tag{16}$$

Where:

j_{M,x_i} is the solute flux under molecular diffusion ($MT^{-1}L^{-2}$)

C is the concentration (ML^{-3})

D_d is the molecular diffusion coefficient (L^2T^{-1})

In the case of transient systems, the flux can be calculated using Flick's second law of diffusion (Fetter and Kreamer, 2022)

$$\frac{\partial C}{\partial t} = -D_d \frac{\partial^2 C}{\partial x_i^2} \tag{17}$$

Typically, the value of D_d for ions is in the order or magnitude of 10^{-9} m^2/s and the coefficient is isotropic. However, in porous media, the diffusion coefficient has a lower value since the chemical species have to move through the pore throats of the interconnected pore network. Consequently, the diffusive flux will be (Sethi and Di Molfetta, 2019)

$$j_{M,x_i} = -n_e D_0 \frac{\partial C}{\partial x_i} = -n_e (D_d \bullet \tau) \frac{\partial C}{\partial x_i} \tag{18}$$

Where:

D_0 is the effective diffusion coefficient (L^2T^{-1})

τ is the tortuosity (-)

The tortuosity is a parameter that describes how the porous structure develops, measuring how much the path between two points in the pore network differs from the shortest line that can connect those two points (da Silva *et al.*, 2022).

2.1.4.2 Advection

During advective transport, solutes move in the aquifer at the same velocity and direction as groundwater. The formula to find the value of the seepage velocity is the one reported in equation (11) (Fetter and Kreamer, 2022). Therefore, the mass flux resulting from the advective transport of chemical species along the horizontal direction, through a cross-sectional area whose effective porosity is known is

$$j_{A,x} = n_e v_x C \tag{19}$$

Where:

$j_{A,x}$ is the advective flux ($MT^{-1}L^{-2}$)

If no diffusive transport processes take place during the solutes movement and the source of chemical species is continuous, then the concentration downstream of the front will be zero, while upstream will be equal to the one at the source. Moreover, the front would be perpendicular to the direction of the average linear velocity (Sethi and Di Molfetta, 2019).

2.1.4.3 Mechanical Dispersion

Mechanical dispersion is a transport mechanism caused by the heterogeneities present in the porous medium that cause variations in the average linear velocity distribution. A velocity component perpendicular to the seepage velocity will also arise, causing the groundwater spread further in the reservoir. This mechanism, like molecular diffusion, can be described with Fick's law (Sethi and Di Molfetta, 2019)

$$j_{C,x} = -n_e D_{C,L} \frac{\partial C}{\partial x} \tag{20}$$

$$j_{C,y} = -n_e D_{C,T} \frac{\partial C}{\partial y} \tag{21}$$

$$j_{C,z} = -n_e D_{C,T} \frac{\partial C}{\partial z} \tag{22}$$

Where:

j_{C,x_i} is the solute flux under mechanical dispersion ($MT^{-1}L^{-2}$)

$D_{C,L}$ is the longitudinal mechanical dispersion coefficient (L^2T^{-1})

$D_{C,T}$ is the transverse mechanical dispersion coefficient (L^2T^{-1})

2.1.4.4 Hydrodynamic Dispersion

Hydrodynamic dispersion is a transport process that combines both mechanical dispersion and molecular diffusion. This is possible since both the mechanisms are described using Fick's law, therefore the formula for hydrodynamic dispersion is (Sethi and di Molfetta, 2019)

$$j_{I,x} = -n_e D_L \frac{\partial C}{\partial x} \tag{23}$$

$$j_{I,y} = -n_e D_T \frac{\partial C}{\partial y} \tag{24}$$

$$j_{I,z} = -n_e D_T \frac{\partial C}{\partial z} \tag{25}$$

$$D_L = D_0 + D_{C,L} \tag{26}$$

$$D_T = D_0 + D_{C,T} \tag{27}$$

Where:

j_{I,x_i} is the solute flux under hydrodynamic dispersion ($MT^{-1}L^{-2}$)

D_L is the longitudinal hydrodynamic dispersion coefficient (L^2T^{-1})

D_T is the transverse hydrodynamic dispersion coefficient (L^2T^{-1})

2.2   Fracture Grouting

As stated before, fracture grouting, also called compensation, is an engineering technology which involves the injection of cement into the discontinuities present in heterogenous geological units to stabilize them and take on the characteristics of homogenous formations (Deng *et al.*, 2018). In addition, highly fractured rocks allow groundwater flow which will result in the erosion of the overlying dam foundations (Liu *et al.*, 2019).

2.2.1   Portland Cement

Portland cement is a material created by taking exact amounts of clay and limestone to high temperatures inside of a kiln. Due to the fact that the raw materials required are not artificial, but natural, the chemical composition of Portland cements produced in different factories and even in different kiln won't be the exact same. Inside the kiln, the high temperature will trigger various chemical reactions among the different minerals constituting the raw materials, which after being pyro-processed are called clinker.

The main compounds that make up the clinker are tricalcium silicate ($SiO_2 \cdot 3CaO$, or C3S), dicalcium silicate ($SiO_2 \cdot 2CaO$, or C_2S), tricalcium alluminate ($Al_2O_3 \cdot 3CaO$, or C3A), and tetracalcium ferroalluminate ($4CaO \cdot Al_2O_3 \cdot Fe_2O_3$, or C_4AF). Apart from these minerals, lower amounts of sodium oxide (Na_2O), potassium oxide (K_2O), and magnesia (MgO) are also present. Based on the type of cement produced and on the raw materials origin, the fraction of each mineral present will vary, for example, the percentage of lime can range from 60% to 70%. The clinker will then have to undergo a griding treatment to get finer particles before water can be added to start the hydration process (Aïtcin, 2016).

2.2.1.1 Portland Cement Hydration

Given that the aim of this study is to analyze portlandite dissolution due to groundwater flow, the latter will be the focus in this paragraph.

The hydration of Portland cement is a series of exothermic chemical reactions that start a few minutes after the addition of water to the clinker and last for a few days, leading to the hardening of the cement paste with an overall increase in mechanical properties. The

hydration process can be divided into five subphases according to the generated heat, as shown Figure 1, during which the four main minerals react at separate instances.
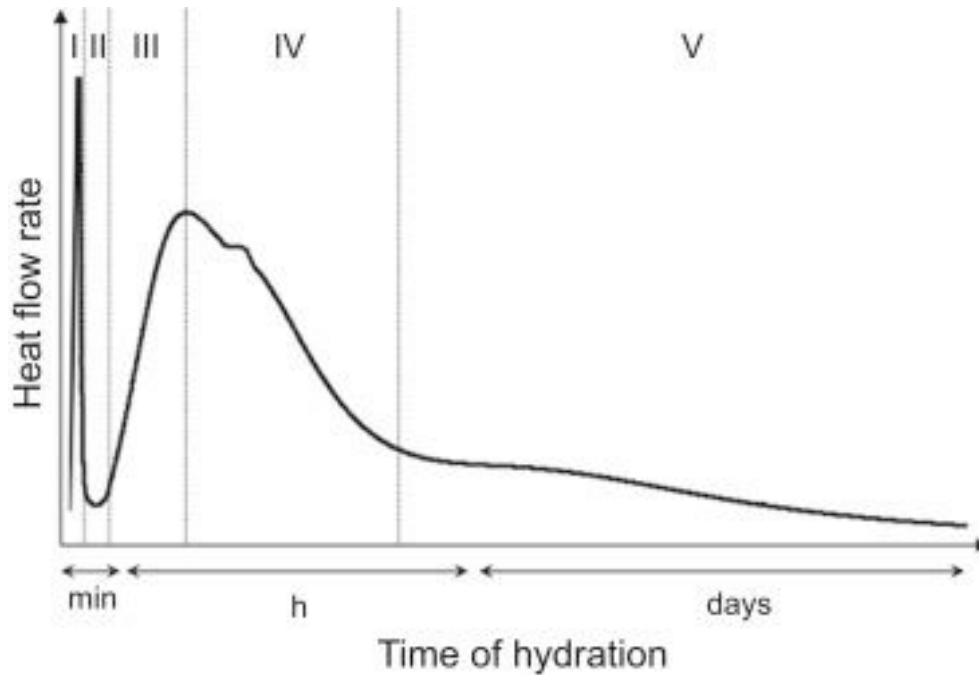

Figure 1: Portland Cement Hydration Stages (Aïtcin, 2016:39)

The formation of portlandite arises from the hydration of C_3S and C_2S, where the first reacts during stages I, III, and IV, while the latter mainly undergoes chemical changes in stage V. The amount produced is relatively high given that tricalcium silicate and dicalcium silicate represent from 20% to 30% of the clinker, and the first is responsible for most of the generation since it contains more CaO molecules. Apart from the calcium oxide hydrate, other minerals called calcium silicate hydrates (C-S-H) are formed (Aïtcin, 2016). These are a class of amorphous compounds with the same chemical make-up but different stoichiometry and morphology, rather than a singular well defined compound. C-S-H gels enhance the durability of the hardened concrete (Marchon and Flatt, 2016). The reaction regarding the formation of these two phases can be represented in simplified form as

$$(C_3S, C_2S) + H_2O = C\text{-}S\text{-}H + portlandite$$
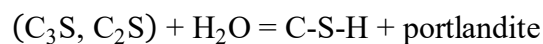
The main benefit of having portlandite in the cement paste is that it raises the pH of pore water, slowing down the degradation of other components present. Besides this, its contribution to the overall strength of the cement is negligible (Aïtcin, 2016).

2.2.1.2 Portland Cement Degradation

Considering the low values of average linear velocity that groundwater has when flowing through cement grout caused by its hydraulic properties, the degradation processes tend to be quite slow. One of these deterioration mechanisms is groundwater dissolution, which can be divided in different steps. Firstly, sodium and potassium hydroxides, present in trace amounts, will be flushed out of the grouted area by groundwater flow. Once those compounds are gone, unreacted portlandite, which maintains the porewater pH at around 12.5, will be broken down into calcium ions and water molecules. When all the $Ca(OH)_2$ is removed, C-S-H gels dissolution will begin, and the pH will decrease. The complete removal of calcium silicate hydrates will depend on the ionic characteristics of groundwater, taking more time if the infiltrating water has high concentration of dissolved ions (Gascoyne, 2002).

3　Data and Methodology

This analysis was carried out using the software COMSOL Multiphysics® version 6.2 for the fluid flow and reactive transport portions, while the concentration of the transported species was determined using the geochemical modelling software PHREEQC. The input data for the elemental composition of both the groundwaters and porewater were taken from SKB working report R-19-11, by Idiart and Shafei (2019).

3.1　Groundwater Modelling

The groundwater model built to carry out this analysis was based on two main modules, one concerning the plain subsurface flow and one for the reactive transport of solutes. The first step in groundwater modelling is to create a simplified and static version of the flow system, known as the conceptual model, which allows to understand how it works. The numerical flow model, a more complex version of the previous study, is built using a steady-state simulation and the results obtained are compared to the conceptual model. If the results are considered acceptable, the simulation process can progress to the transient state study, in which the values calculated by the software will vary both over space and time. in the transient simulation, the groundwater flow will be coupled with the reactive transport of solutes, which as Fetter and Kreamer (2022) remember, add an equation that accounts for the variations in the chemical composition of groundwater following the chemical reactions.

3 – DATA AND METHODOLOGY

COMSOL Multiphysics® is based on Finite-Elements Method (FEM) approach, meaning that it divides the modelled geometry into as many tetrahedral-shaped elements as the resolution is set to be. These elementary units are interconnected at their vertices, where the software will calculate the values of the variables considered in the analysis and then an interpolation process will be performed to find the values in the remaining parts of the domain (Fetter and Kreamer, 2022). By doing so, the software can simplify the equations from their original form, which is of partial differential equations (PDEs), by approximating them as numerical equations whose solution can be found in a simpler way (COMSOL, 2016).

However, PDEs alone are not sufficient to solve groundwater flow problems, it is necessary to include additional information concerning the state of the domain before the beginning of the simulation, and how it relates to the adjacent environment that is not included in the model. This is done by specifying the initial conditions (IC) and boundary conditions (BC) (Sethi and Di Molfetta, 2019). An example of IC for the flow model using Darcy's law could be setting the hydraulic head values in the domain. At the same time, for the transport part usually the concentration of each species is given at time zero (COMSOL, 2018). As for the BC, there are five different types to choose from depending on the processes that will be analyzed, only three will be discussed in this paragraph. The first type, known as Dirichlet BC, prescribes the numeric quantity of a dependent variable on the edge of the domain, either as a constant or as a function of time and/or space. For example, the hydraulic head or the concentration of solutes outside of the model area. The second type, or Neumann BC, defines the derivative of a dependent variable on the boundary once again as a constant or as a function of space and/or time, like a water or mass flux coming in or out of the considered region. A special type of Neumann BC is the no-flow condition, where the flux is set to zero to identify impermeable areas in the domain. Lastly, the Robin BC is the third type and it consist of a linear combination of the first and second type BC (Jazayeri and Werner, 2019).

For this analysis, a period of 20 years has been considered, with an output every 0.05 years. When solving a transient model, COMSOL Multiphysics® changes dynamically the time step sizes to respect the relative tolerance. When the time-dependent solver comes across sharps gradients the time steps will decrease, while they are increased when

the opposite is true. The initial time step is estimated on the base of the total time specified. This can sometimes lead to convergence problems and a possible solution is for the user to choose an initial time step size, which in this case was 0.001 seconds. The porosity and hydraulic conductivity field were calculated in post-processing.

3.2 Model Geometries

In this thesis, the calculations were computed for two different geometries, the first representing a two-dimensional infinite fracture while the second depicted a three-dimensional fracture. The 3D fracture geometry, shown in Figure 2, was taken by Zou *et al.* (2017), while the 2D one has been obtained by selecting a section of the previous one.
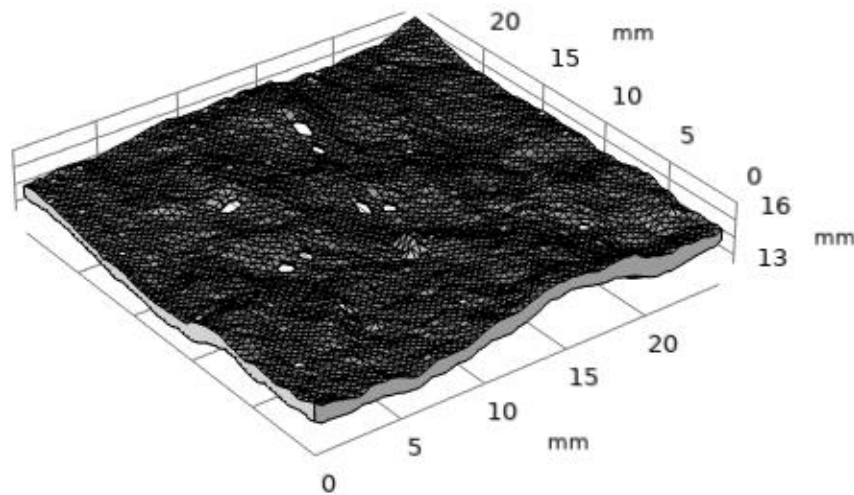

Figure 2: Rough Fracture Geometry

The geometry was created using a laser scanner on a naturally occurring fracture in a granite sample measuring 24.8 mm in width and length. To reproduce a realistic fracture a 1.0 mm shear displacement was applied along the direction of groundwater flow, the y-axis. This displacement generated a heterogenous aperture in the geometry, resulting in multiple contact points between the upper and lower surfaces, as Figure 3 shows (Zou *et al.*, 2017). The distribution of the fracture aperture and the resulting contact points can be seen in Figure 4. This non-uniformity of the geometry is interesting cause it could affect the path on which subsurface water moves and therefore the overall final results of the study, compared to the ones obtained from a fracture with a constant aperture.
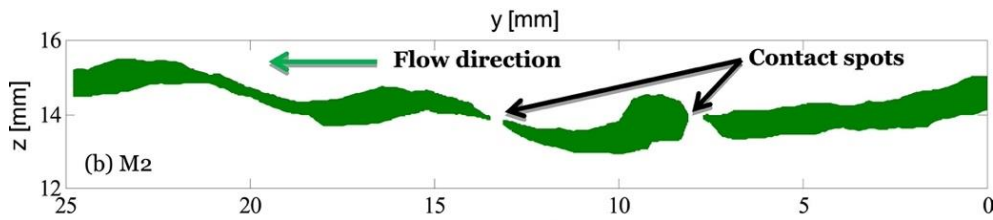
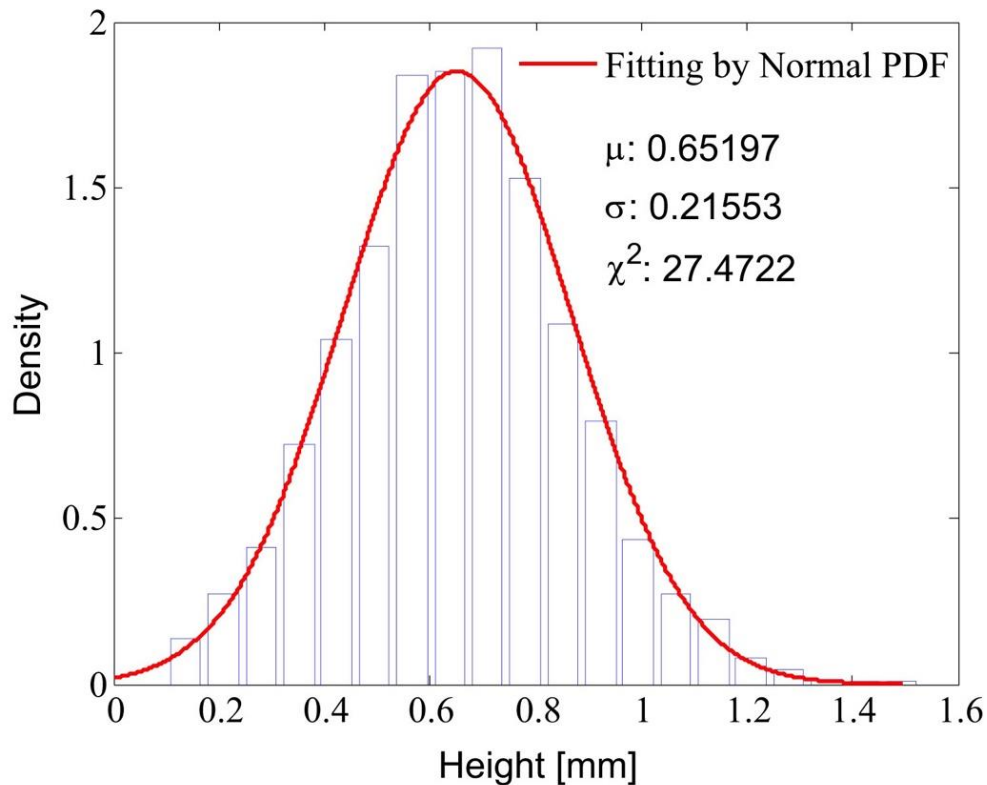*Figure 3: Fracture Aperture at x = 12.5 mm (Zou et al., 2017:35)*

Figure 4: Fracture Aperture Distribution (Zou et al., 2017:36)

The two-dimensional fracture was obtained from the previous geometry by selecting a section along the yz plane. Similar to the previous case, the aperture height distribution is not homogeneous. However, in this instance no contact points are present as they wouldn't allow for the creation of a single domain model, causing obstructions that wouldn't allow the groundwater to flow at all. This geometry was a useful tool as it allowed to carry out the simulation making sure that the model behaviour was accurate before moving on to the more computationally demanding 3D model. The two-dimensional geometry is shown in Figure 5.

Figure 5: 2D fracture geometry

3.3   Numerical Model

3.3.1 Groundwater Flow Model

As reported in the previous sections, the fracture was assumed to be placed under a dam and filled with concrete grout to enhance the overall rock's mechanical properties and prevent the groundwater flow from eroding the foundations. The hydraulic properties of the concrete grout were the ones used by Idiart and Shafei (2019), with a porosity value of 0.11 and hydraulic conductivity of $8.30 \cdot 10^{-10}$ m/s. The groundwater flow has been simulated using Darcy's law physics. A value of hydraulic head equal to 6 meters was chosen as the IC in the entire flow domain. For the BC, two Dirichlet constant head conditions have been imposed on the left and right boundaries of the domain. Specifically, the right one was set to a constant value of 6 meters, while the left one was adjusted to obtain a hydraulic gradient of 0.01. For all the remaining boundaries, a Neumann no-flow BC has been applied, ensuring that no groundwater would be able to cross those borders. The different kinds of boundary conditions are shown in Figure 6. A constant head condition is assigned to both the inflowing and outflowing boundaries, whereas the blue

ones are assigned no flux conditions. The same goes for the 2D geometry, as it's derived from the 3D one.
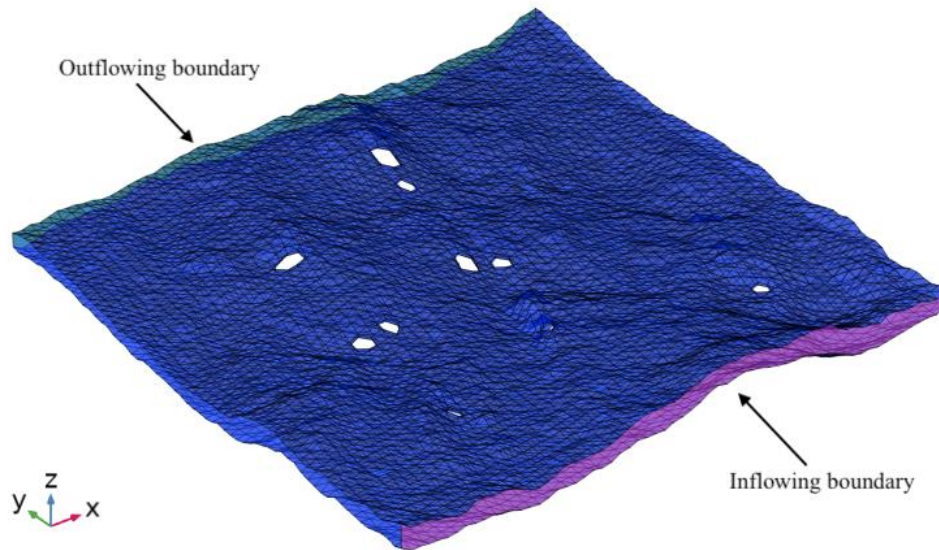

Figure 6: Different types of boundary conditions shown on the three-dimensional geometry.

3.3.2 Transport Model

The transport portion of the model was built using the Transport of Diluted Species in Porous Media physics (tds) interface, coupled with the fluid flow interface through the velocity field. The chemical species concentrations used in the transport model were obtained by performing speciation simulations in PHREEQC, the CEMDATA18.11 (Lothenbach *et al.*, 2019) database was chosen as it describes chemical reactions in cementitious materials.

The Transport of Diluted Species in Porous Media module considered both advection and diffusion as the transport mechanisms. The diffusion coefficient for all the species was set to $3.50 \cdot 10^{-12}$ m/s, meaning that the diffusive process was slow. This was confirmed by the Péclet number, which had a value of 40, meaning that the advection was the main transport mechanism in the simulation. Two distinct groundwater compositions were considered. The porewater and groundwater compositions and the initial amount of

portlandite present in the domain, taken from Idiart and Shafei (2019), are shown in Table 1 and Table 2.

The IC in the Transport of Diluted Species in Porous Media corresponded to the values listed in Table 3. For BC, a Concentration BC was applied to the inflowing boundary, while an Outflow one was applied to the outflowing one, ensuring continuity with the groundwater flow direction. The Concentration BC is a kind of Dirichlet BC, while the Outflow is a Neumann one. The species concentrations used for the Concentration node are reported in Table 4. The remaining boundaries are once again defined as no-flow boundaries, blocking the mass transport through these surfaces.

Table 1: Initial porewater composition, from Idiart and Shafei (2019)

Initial porewater composition	
pH [-]	12.951
Temperature [°C]	25.0
Elements	**Concentration [mol/kg$_W$]**
Al	$4.099 \bullet 10^{-5}$
C	$1.827 \bullet 10^{-5}$
Ca	$3.826 \bullet 10^{-3}$
Cl	$5.124 \bullet 10^{-5}$
K	$8.747 \bullet 10^{-2}$
Na	$2.667 \bullet 10^{-2}$
S(6)	$4.099 \bullet 10^{-5}$
Si	$4.449 \bullet 10^{-5}$

Table 2: First kind of inflowing groundwater chemical composition, from Idiart and Shafei (2019)

First inflowing groundwater composition	
pH [-]	8.64
Temperature [°C]	25.0
Elements	**Concentration [mol/kgw]**
Al	$1.210 \cdot 10^{-6}$
C	$6.910 \cdot 10^{-4}$
Ca	$5.260 \cdot 10^{-4}$
Cl	$4.530 \cdot 10^{-3}$
K	$7.600 \cdot 10^{-5}$
Mg	$1.480 \cdot 10^{-4}$
Na	$4.790 \cdot 10^{-3}$
S(6)	$3.730 \cdot 10^{-4}$
Si	$1.420 \cdot 10^{-4}$

Table 3: Species Concentration in Porewater

Concentration of each species in porewater	
Species	**Concentration [mol/m^3]**
H$_2$O	$5.551 \cdot 10^4$
H$^+$	$1.119 \cdot 10^{-10}$
OH$^-$	$1.049 \cdot 10^2$
Ca^{2+}	2.231

Ca(OH)₂	$1.03598 \bullet 10^3$

Table 4:Species Concentration in Inflowing Groundwater

Concentration of each species in first inflowing groundwater	
Species	**Concentration [mol/m³]**
H₂O	$5.551 \bullet 10^4$
H⁺	$2.291 \bullet 10^{-6}$
OH⁻	$4.704 \bullet 10^{-3}$
Ca²⁺	$4.985 \bullet 10^{-1}$
Ca(OH)₂	0.0

3.3.3 Post-processing

After several attempts, it wasn't possible to develop a model in which the porosity and hydraulic conductivity evolved dynamically at every time step following the portlandite concentration changes, due to convergence problems. As a result, it was decided to compute the variations in porosity and hydraulic conductivity in post-processing, allowing for a more accurate model. The relationships used to compute the two properties were the ones provided by Idiart and Shafei (2019), which relate the porosity, and therefore the hydraulic conductivity, to the concentration of portlandite present in the domain:

$$\varphi = \varphi_0 + \varphi_0 \bullet \left(C_{0,CH} V_{m,CH} - C_{CH} V_{m,CH} \right) \qquad (28)$$

$$K(\varphi) = K(\varphi_0) \bullet \frac{(1 - \varphi_0)^2}{\varphi_0^3} \frac{\varphi^3}{(1 - \varphi)^2} \qquad (29)$$

Where:

φ is the porosity at the i-th time step (-)

φ_0 is the initial porosity (-)

$C_{0,CH}$ is the initial portlandite concentration (NL^{-3})

C_{CH} is the portlandite concentration at the i-th time step (NL^{-3})

$V_{m,CH}$ is the portlandite molar volume (L^{3}N^{-1})

$K(\varphi)$ is the hydraulic conductivity at the i-th time step (LT^{-1})

$K(\varphi_0)$ is the initial hydraulic conductivity (LT^{-1})

Even though this approach didn't reflect the complex mechanisms of these processes, it allowed to carry out the analysis without convergence difficulties.

3.3.4 Meshing

The meshing process enables COMSOL Multiphysics® to divide the geometry into finite elements with variable resolution so that the software can compute the PDEs to effectively solve the problem. The number of elements present in the model depends on their size. The latter influences their quality as well. All these factors will impact the memory requirements and, therefore, the computational time of the simulation (COMSOL, no date). The quality of mesh elements can range from 0 to 1, and usually, values equal to 0.1 or lower are considered not acceptable (Gothäll, 2022).

For the two-dimensional model an "Extra-fine" mesh was built, while for the three-dimensional one a "Finer" mesh had to be used to lower the computational requirements otherwise necessary for higher resolutions. The meshes for the two-dimensional and three-dimensional geometries can be seen respectively in **Error! Reference source not found.** and **Error! Reference source not found.**. The average element quality for the first one is 0.6694, while for the second one is 0.6393.

Figure 7: Two-dimensional model mesh
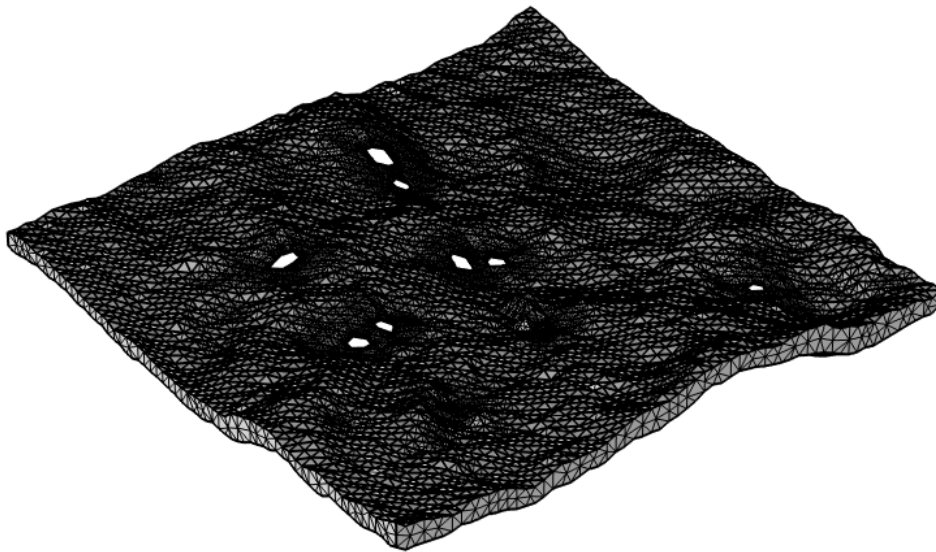
Figure 8: Three-dimensional model mesh

4   Results

For both the two-dimensional and three-dimensional models, a steady-state simulation was first run to obtain the correct values of concentration of the four species in the domain. This step was important to ensure that the species distribution was constant across the domain. The results from these steady-state models were then defined as initial conditions in the time-dependent study. By doing so it was possible to avoid problems regarding inconsistent initial values (COMSOL, no date) and therefore improving convergence.

4.1   Two-dimensional Model

4.1.1 Steady-state Simulation

The hydraulic head distribution resulting from the stationary simulation shown in Figure 9, vary from a value of 6 meters on the right boundary to a value of 5.9975 meters on the left boundary, resulting in a hydraulic gradient equal to 0.01. This gives rise to the velocity distribution in Figure 10, where the highest values of velocity are in correspondence of those areas where the fracture aperture is smaller. Vice-versa, where the aperture is higher and sharp corners are present the velocity takes lower values, manifesting the effects that the irregular geometry has on the groundwater flow.
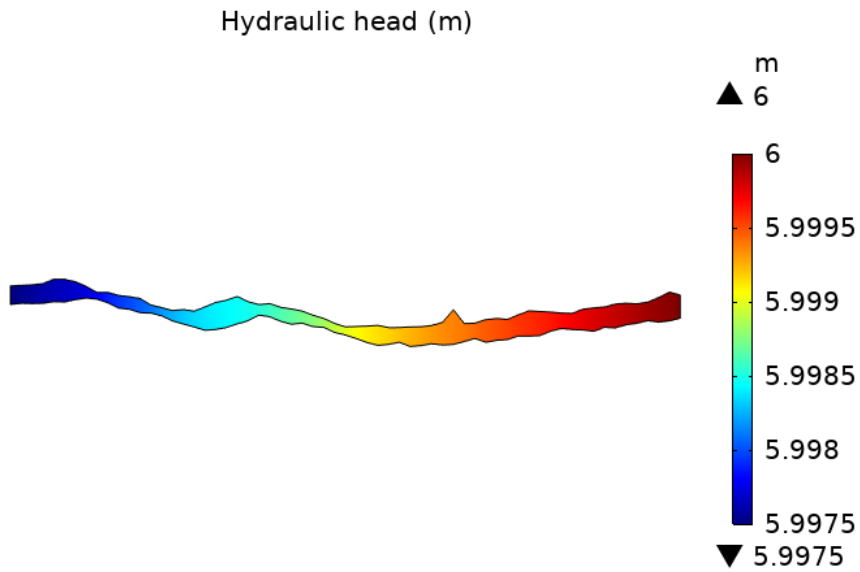
Hydraulic head (m)

Figure 9: Steady-state results showing the hydraulic head in the two-dimensional domain
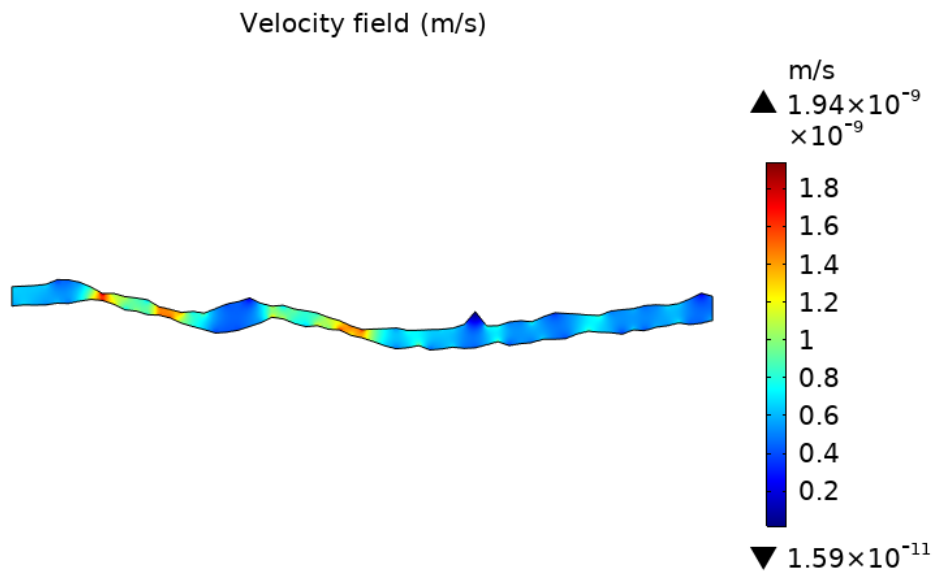
Velocity field (m/s)

Figure 10: Steady-state results showing the velocity field in the two-dimensional domain

By the end of the simulation, the concentration of the four chemical species becomes uniform across the whole domain. Starting from an initial value of 10 mol/m^3 for all compounds, the final concentrations match the ones obtained using PHREEQC, which are listed in Table 3, demonstrating that after a long time an equilibrium is reached and the amount of chemicals present in the domain stabilizes and conforms to the one outside

the area of study. Figure 11, Figure 12, Figure 13, and Figure 14 show the molarities for the different species.

Portlandite concentration (mol/m^3)
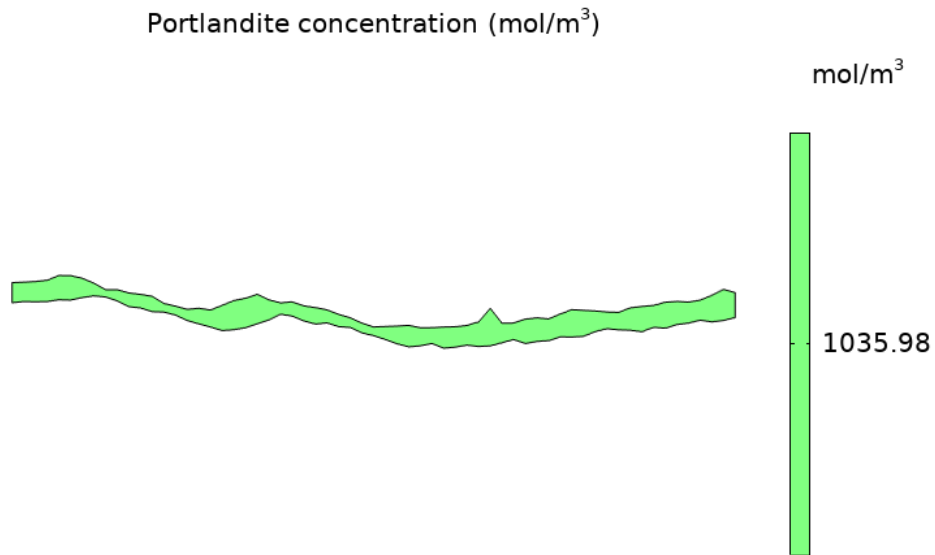
Figure 11: Steady-state simulation result showing Portlandite concentration.

Ca+2 concentration (mol/m^3)
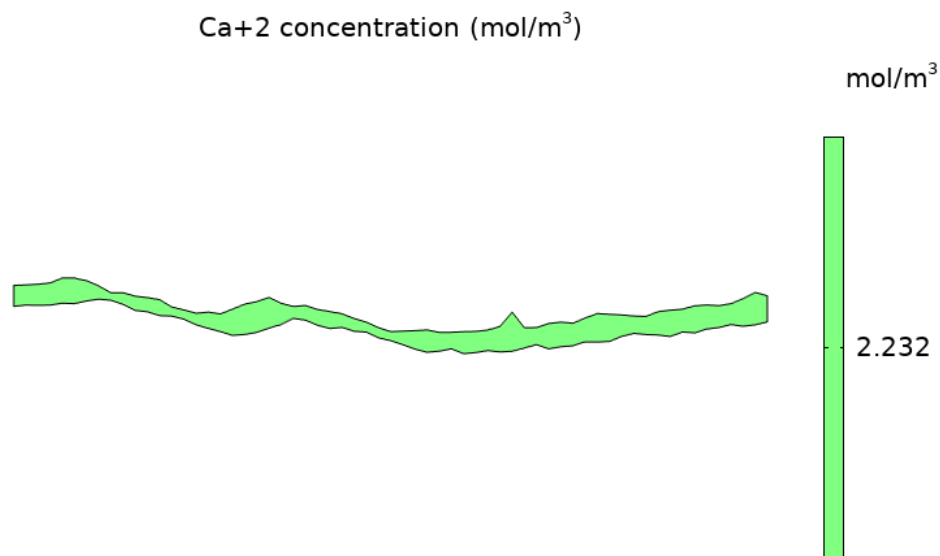
Figure 12: Steady-state simulation result showing calcium ions concentration.

H+ concentration (mol/m^3)
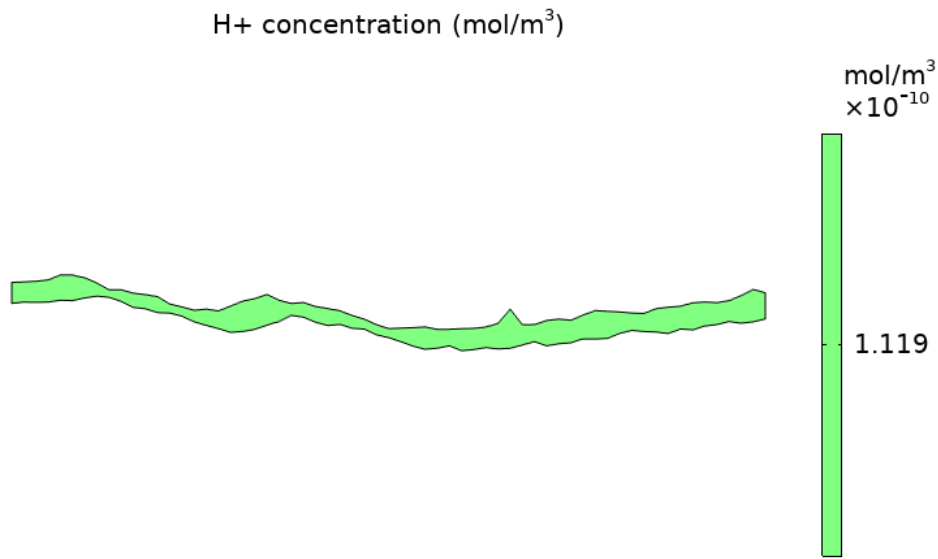
Figure 13: Steady-state simulation result showing hydrogen ions concentration.

OH- concentration (mol/m^3)
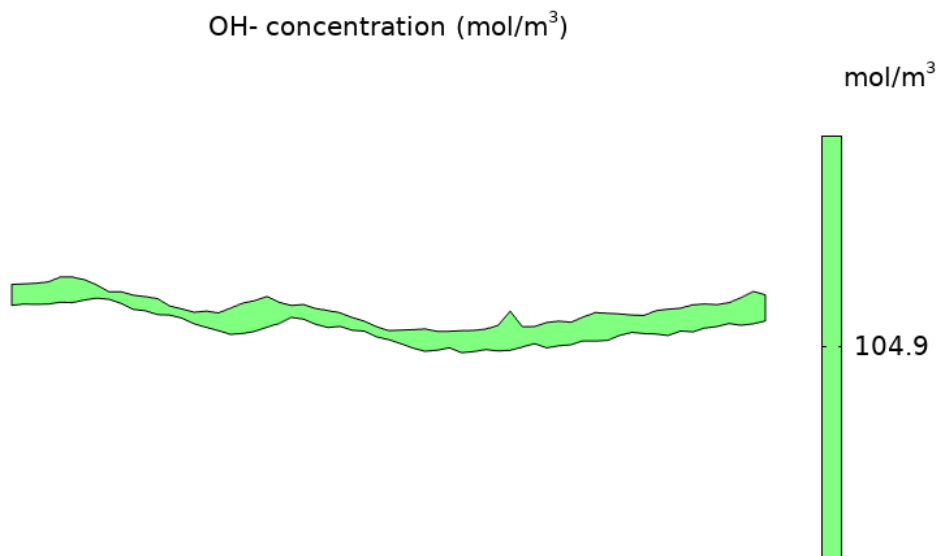
Figure 14: Steady-state simulation result showing hydroxide ions concentration.

4.1.2 Time-dependent Simulation

Figure 15 to Figure 18 show the concentration distributions at the end of the time-dependent simulation. At time zero, the molarity of each chemical species is equal to the steady-state results. The images show the mass transport process from left to right, which

follows the hydraulic head distribution and velocity field. Close to the left boundary, where the Dirichlet BC was applied, the concentration of each species assumes the expected value but not in the rest of the domain, where it takes values closer to the initial ones as the displacement front moves forward.

A longer time frame should have been considered to reach a constant value of molarity everywhere, as in the stationary simulation.
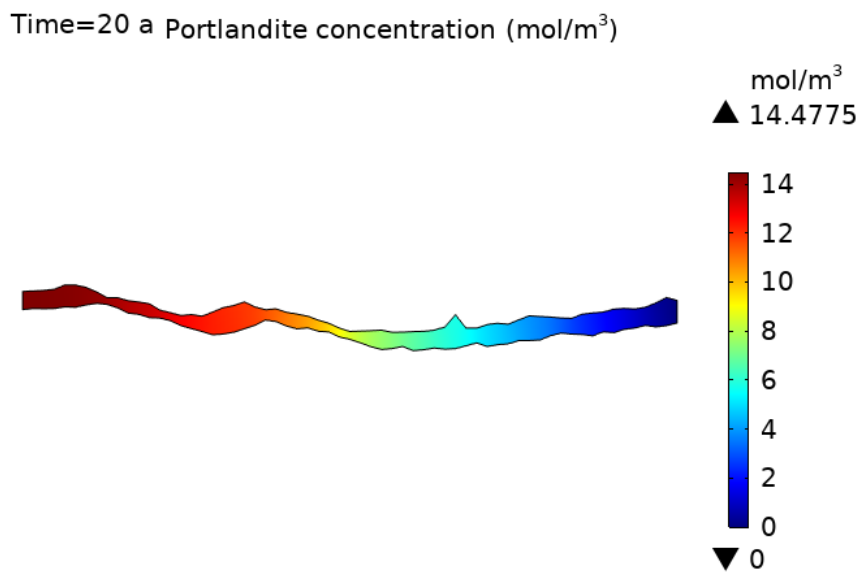
Figure 15: Time-dependent simulation results after 20 years showing Portlandite concentration.

Time=20 a   Ca+2 concentration (mol/m^3)

mol/m^3
▲ 0.5227

0.52
0.515
0.51
0.505
0.5

▼ 0.4985
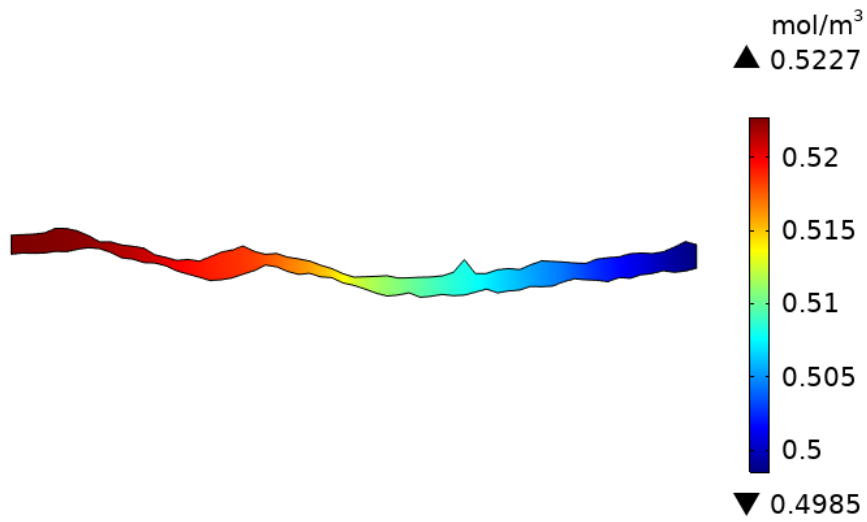
Figure 16: Time-dependent simulation results after 20 years showing Calcium ions concentration.

Time=20 a   H+ concentration (mol/m^3)

mol/m^3
▲ 2.291×10^{-6}
×10^{-6}

2.29
2.285
2.28
2.275
2.27
2.265
2.26

▼ 2.259×10^{-6}
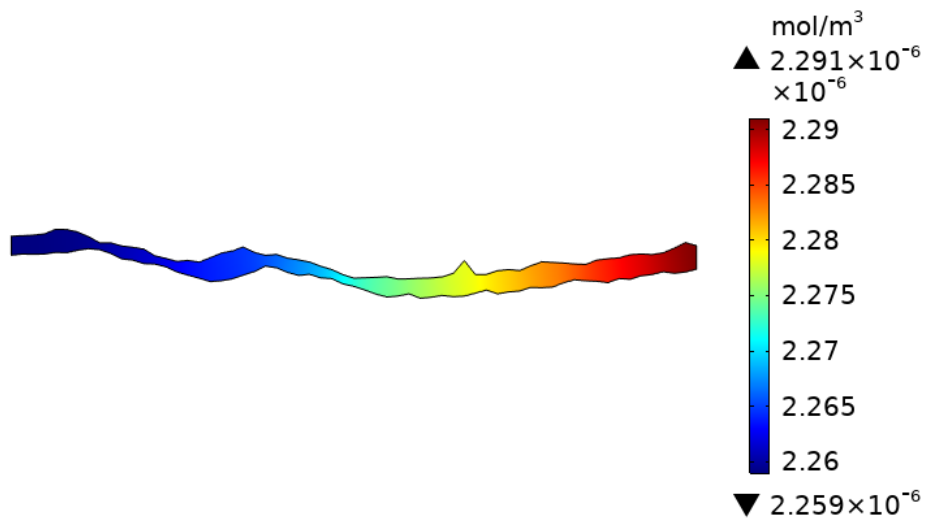
Figure 17: Time-dependent simulation results after 20 years showing hydrogen ions concentration.

Time=20 a   OH- concentration (mol/m^3)

mol/m^3
▲ 1.471
×10^{-3}

1400
1200
1000
800
600
400
200

▼ 4.704×10^{-3}
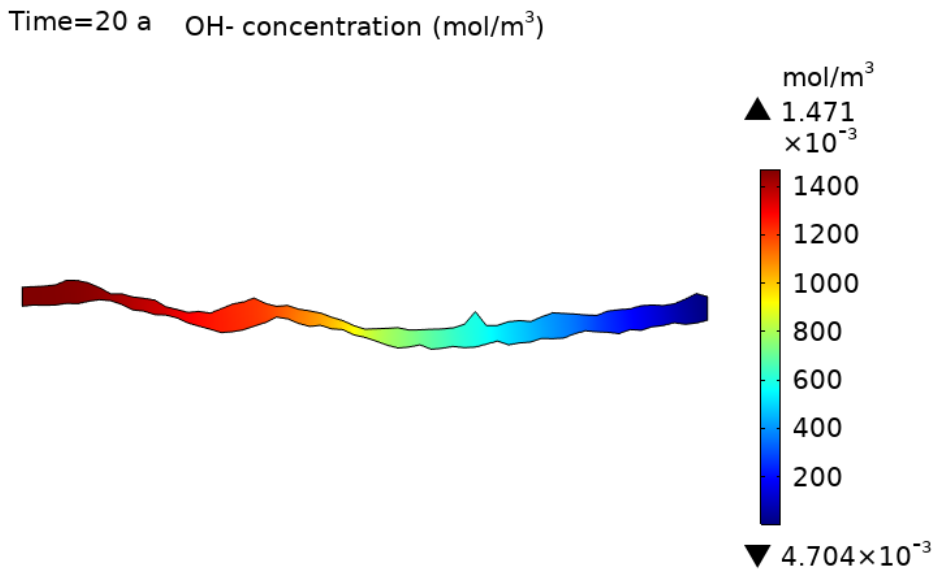
Figure 18: Time-dependent simulation results after 20 years showing hydroxide ions concentration.

To better see how the concentrations of the four compounds change over time, reference can be made to Figure 19, Figure 20, Figure 21, and Figure 22. Each one of the plots refers to the same four evaluation points, where point one coincides with the outflow boundary and points two to four are progressively closer to the inflowing boundary. The variation in molarity gets faster the closer the points are to the inlet boundary, confirming what was previously shown from Figure 15 to Figure 18. A similar concept is shown in Figure 23, Figure 24, Figure 25, and Figure 26, which report the values of concentration across the direction of groundwater flow at time intervals of five years. The discontinuity in the plots is because it wasn't possible to define a cut line able to intersect the domain at every point due to its geometric irregularities. The sharpest gradient in concentration is at time zero when the initial values are constant everywhere except for the left boundary, where the concentration constraint is imposed. As time goes by, the plots get smoother and tend towards the molarity values of the infiltrating solution, which the points closer to zero on the x-axis are the first to approach.

The highest impacts of the degrading processes on the grouting materials are therefore expected in the proximity of the inflow area, while their magnitude will decrease as the displacement front is approached.
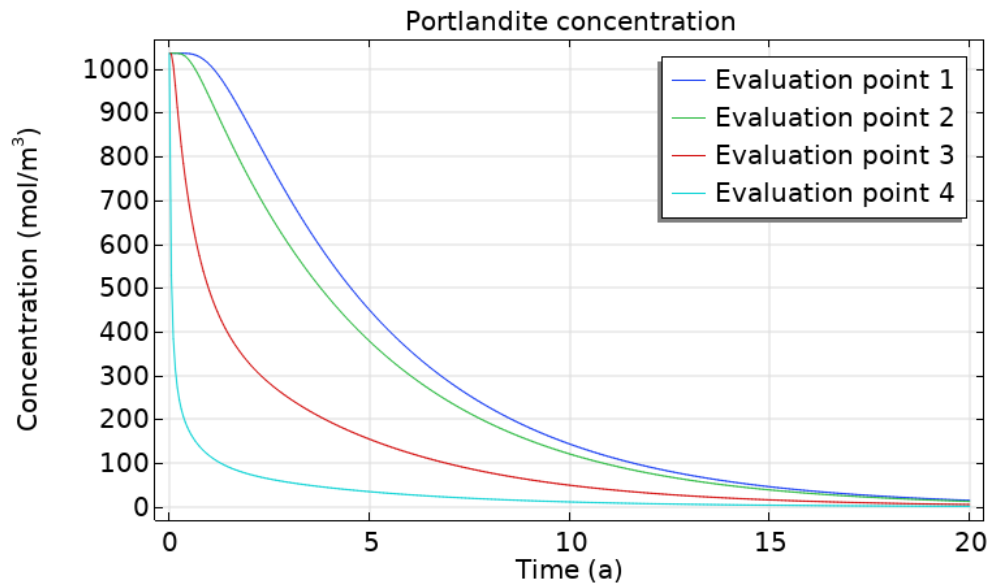
Figure 19: Evolution of the concentration in time at four different points for Portlandite.
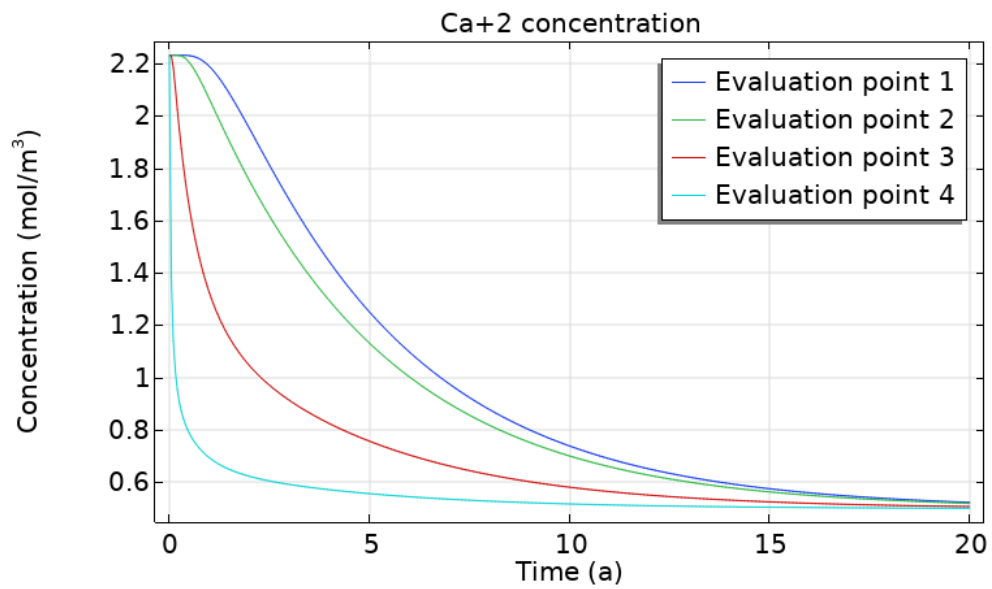
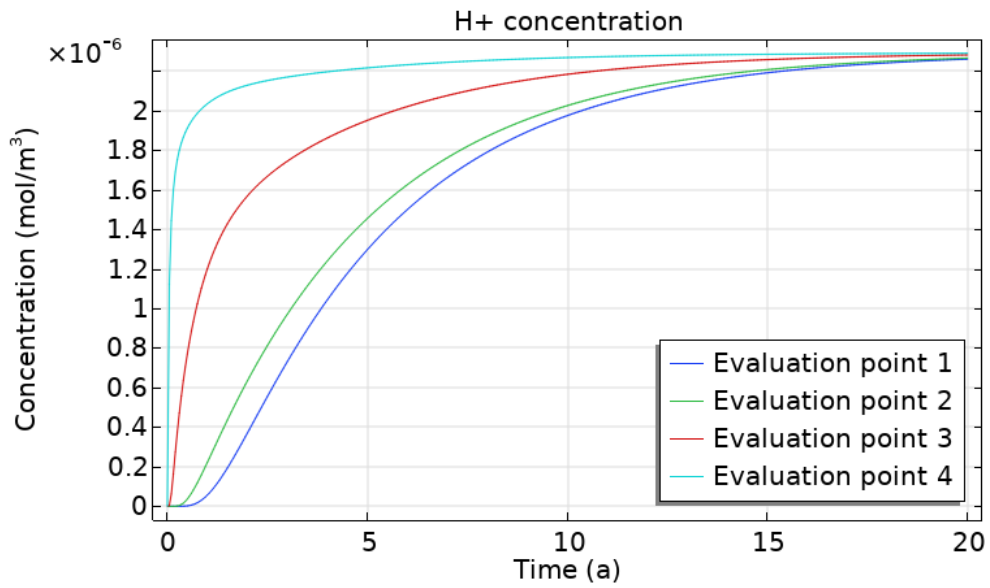*Figure 20: Evolution of the concentration in time at four different points for calcium ions.*

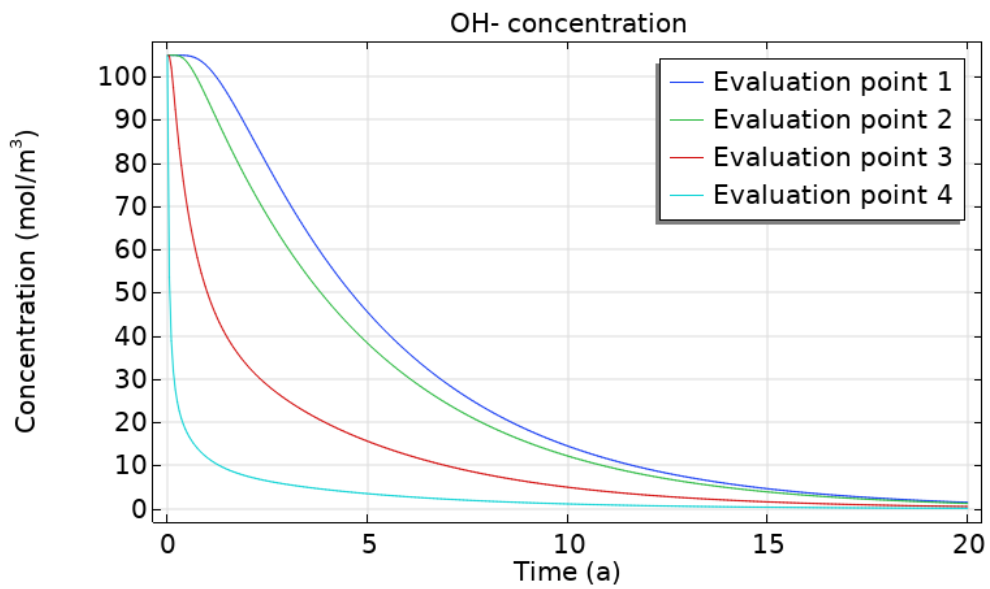*Figure 21: Evolution of the concentration in time at four different points for hydrogen ions.*

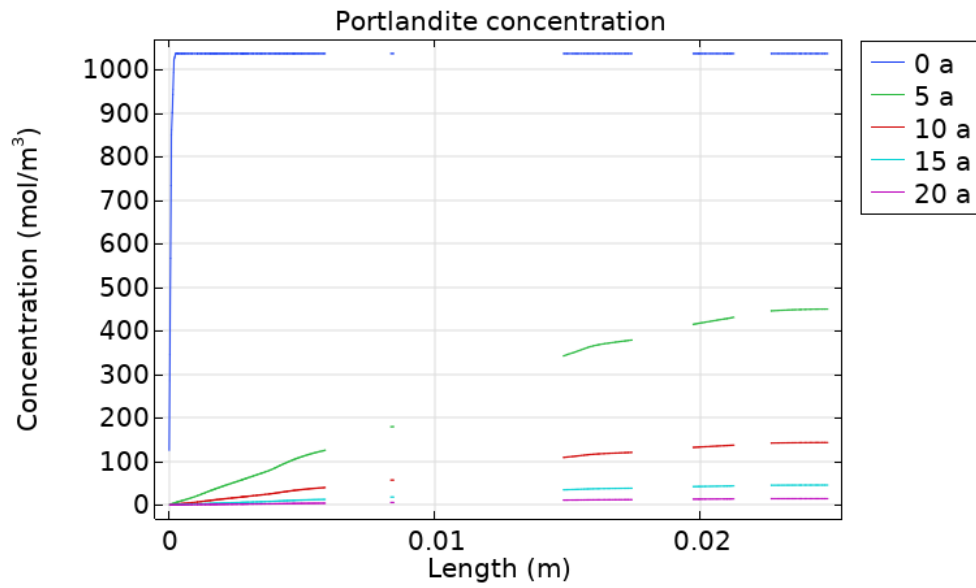*Figure 22: Evolution of the concentration in time at four different points for hydroxide ions.*

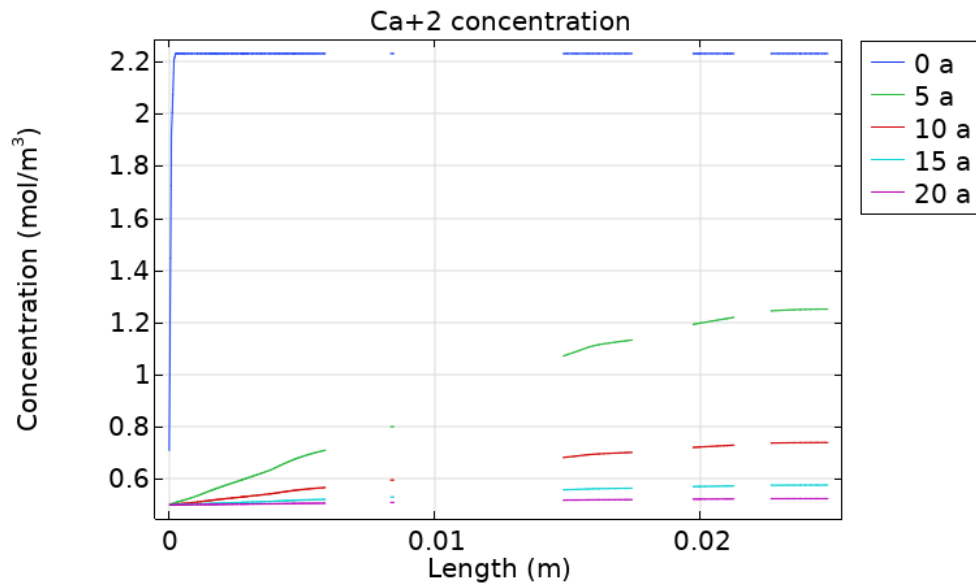*Figure 23: Concentration values over the length of the domain at different output times for Portlandite.*

Figure 24: Concentration values over the length of the domain at different output times for calcium ions.
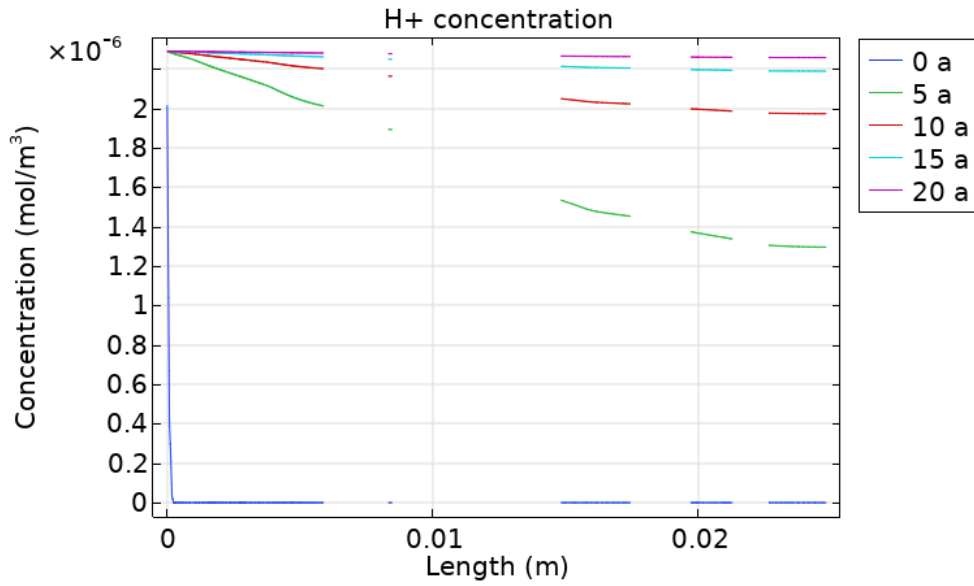
Figure 25: Concentration values over the length of the domain at different output times for hydrogen ions.
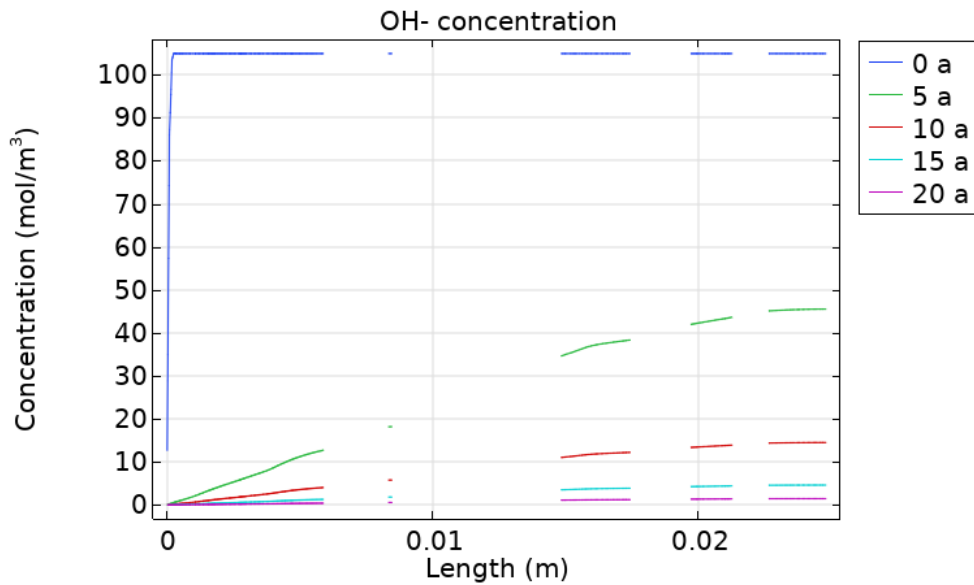
Figure 26: Concentration values over the length of the domain at different output times for hydroxide ions.

Figure 27 and Figure 28 show the pH values in the domain at the beginning of the time-dependent simulation and by the end of it. Initially, the pH value is uniform at 12.951 across the entire domain, except for the left boundary where the infiltrating solution will enter. By the end of the computation, the pH values decrease and range from 8.64 to 8.65.

These results meet expectations, as they coincide with the values reported respectively in Table 1 and Table 2.

Figure 29 and Figure 30 show the variation of pH over time and space. As can be seen, the change over time is rapid at all evaluation points, reaching values lower than nine as early as five years after the simulation began. Moreover, the variation along the length is also pronounced, shifting from the strong gradient at the beginning of the simulation to a much smoother and more uniform distribution already at the second time plotted.
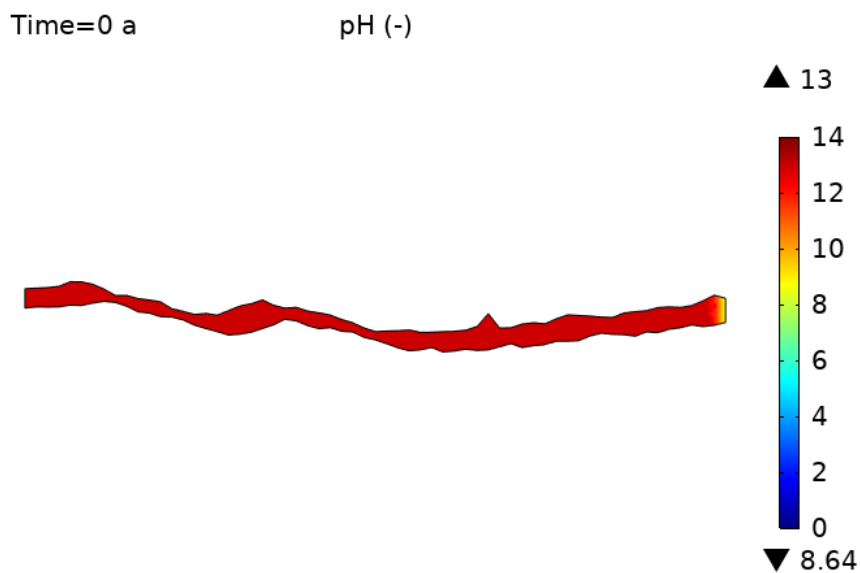
Figure 27: pH values in the whole domain at time 0.

Time=20 a   pH (-)
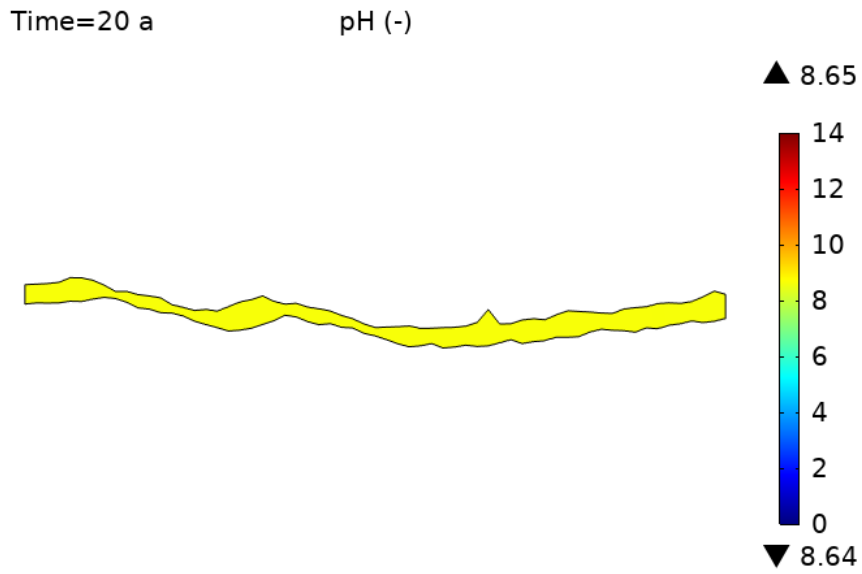
Figure 28: pH values in the whole domain after 20 years.
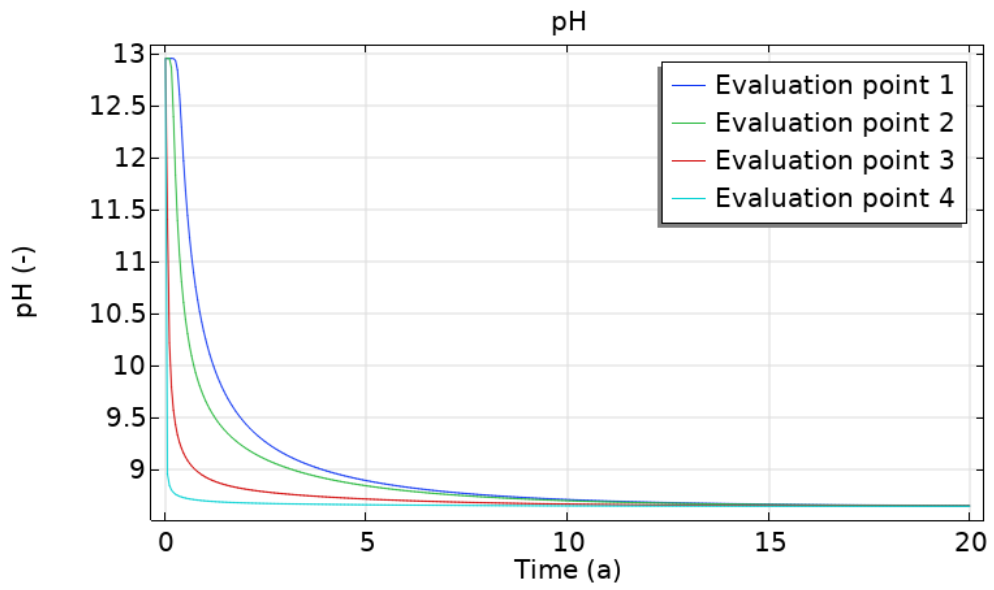
Figure 29: pH variation in time at four different points in the domain.
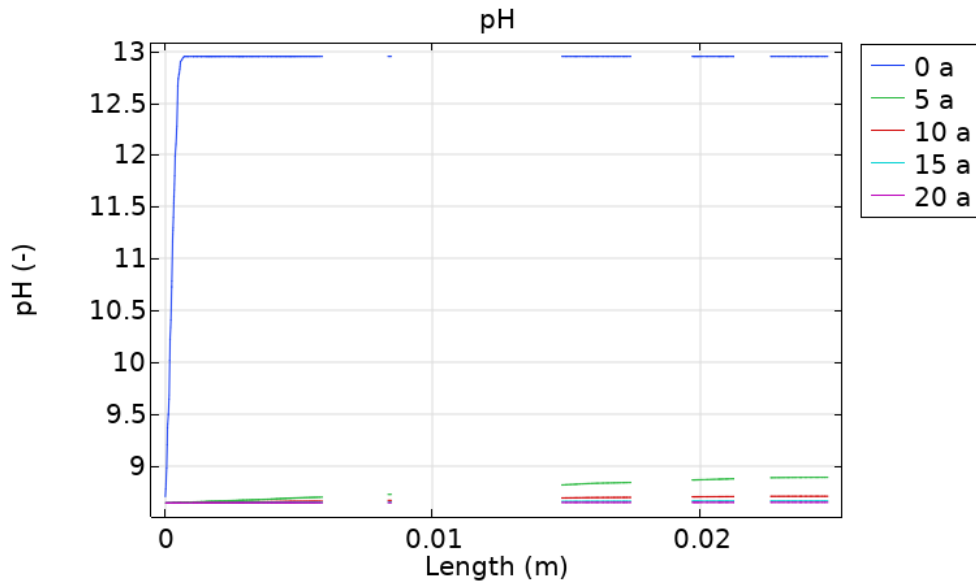
Figure 30: pH values over the length of the domain at different output times.

Finally, the changes in porosity and hydraulic conductivity have been computed based on the equations in Paragraph 3.3.3. The porosity depends on the amount of portlandite present in the domain, and the hydraulic conductivity is a function of porosity. Therefore, as reported in Figure 31 and Figure 33, at time zero, the values obtained match those used as input for the model.

After twenty years, as the concentration of portlandite decreases, the two properties increase in magnitude, reaching values that range from 0.1137 to 0.1138 for the porosity and from $9.09 \bullet 10^{-10}$ m/s to $9.10 \bullet 10^{-10}$ m/s for the hydraulic conductivity, respectively shown in Figure 32 and Figure 34. As can be seen from Figure 35 to Figure 38, what was expected was confirmed: the most significant impacts of the degradation process took place near to the left-side boundary, especially in the first 10 years of the simulation.
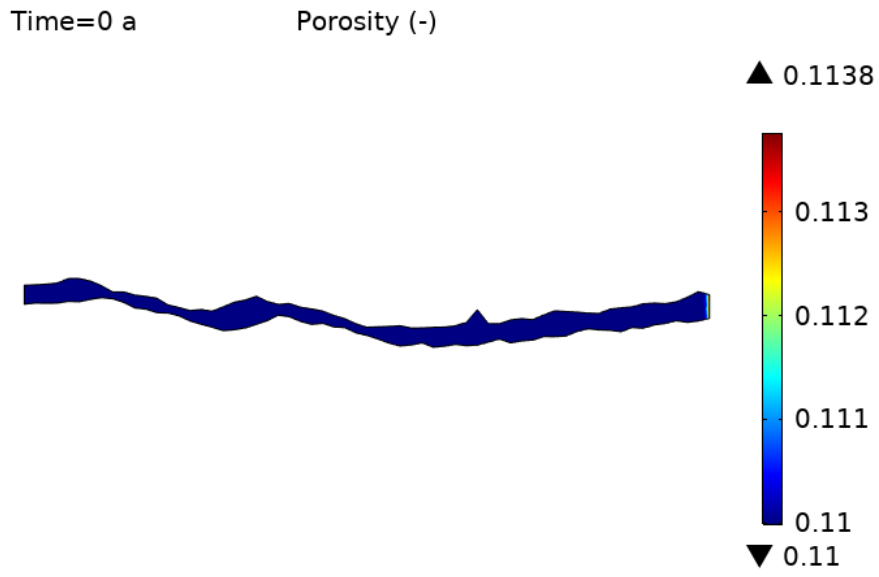
Time=0 a　　　　　Porosity (-)

Figure 31: Porosity values at the beginning of the simulation.
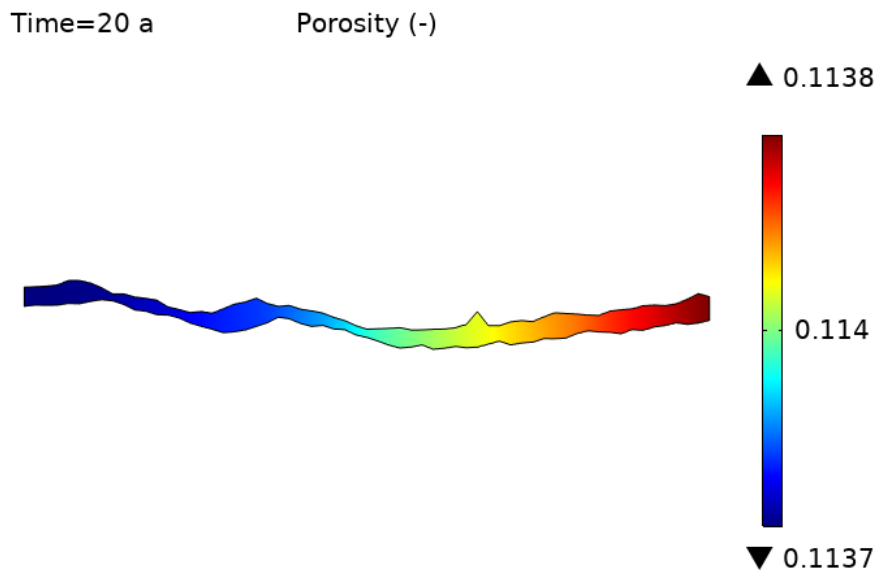
Time=20 a　　　　　Porosity (-)
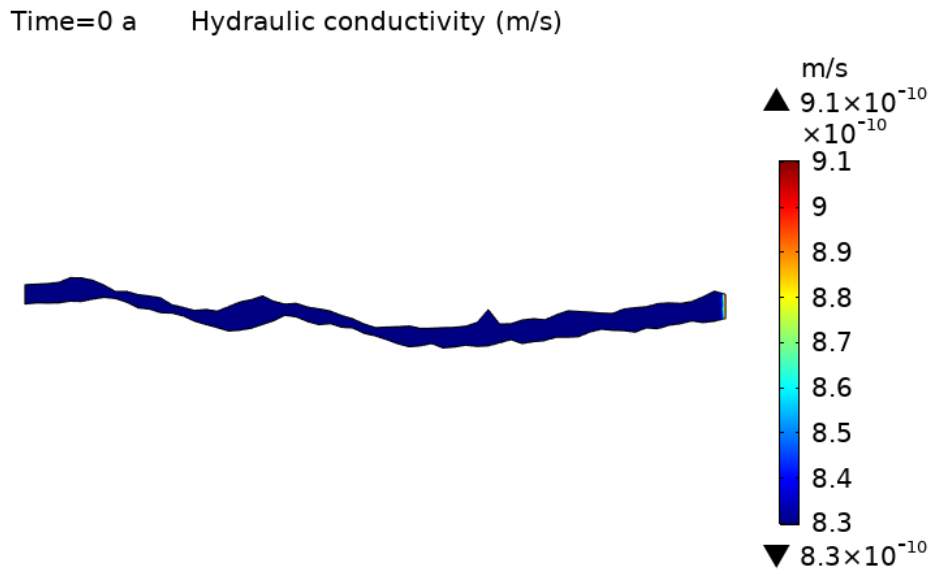

Figure 32: Porosity values after 20 years.

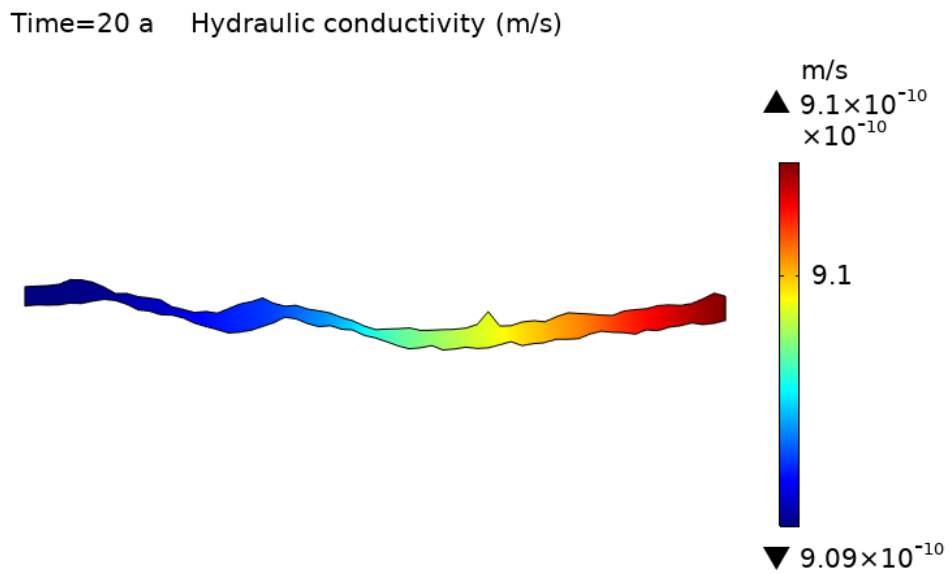*Figure 33: Hydraulic conductivity values at the beginning of the simulation.*

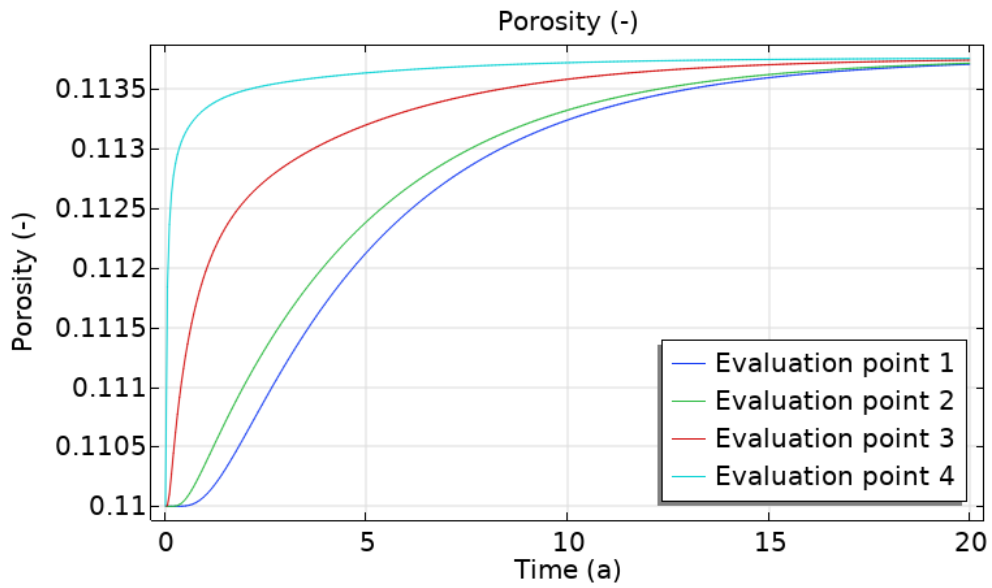*Figure 34: Hydraulic conductivity values after 20 years.*

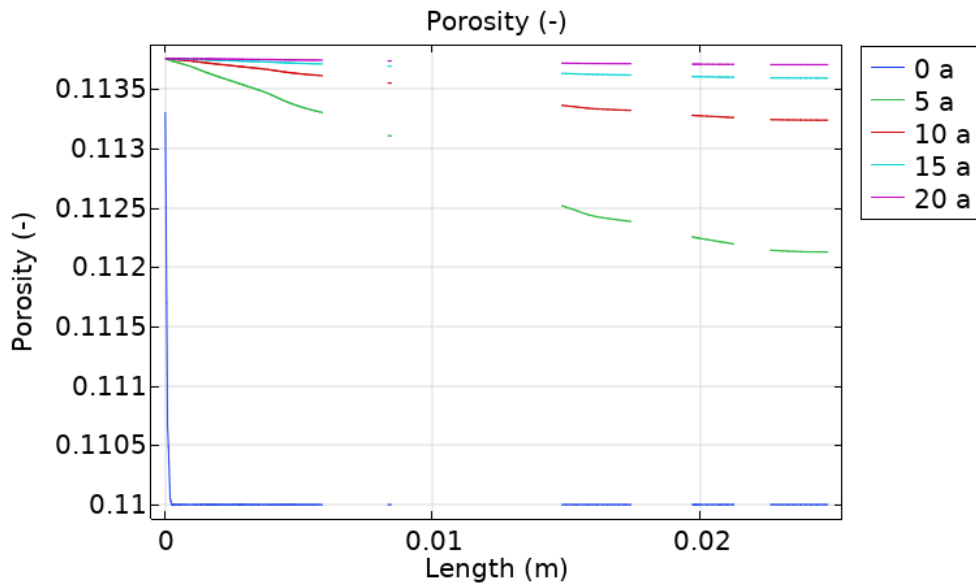*Figure 35: Variation of porosity in time at four different points.*

Figure 36: Porosity values over the length of the domain at four different output times.
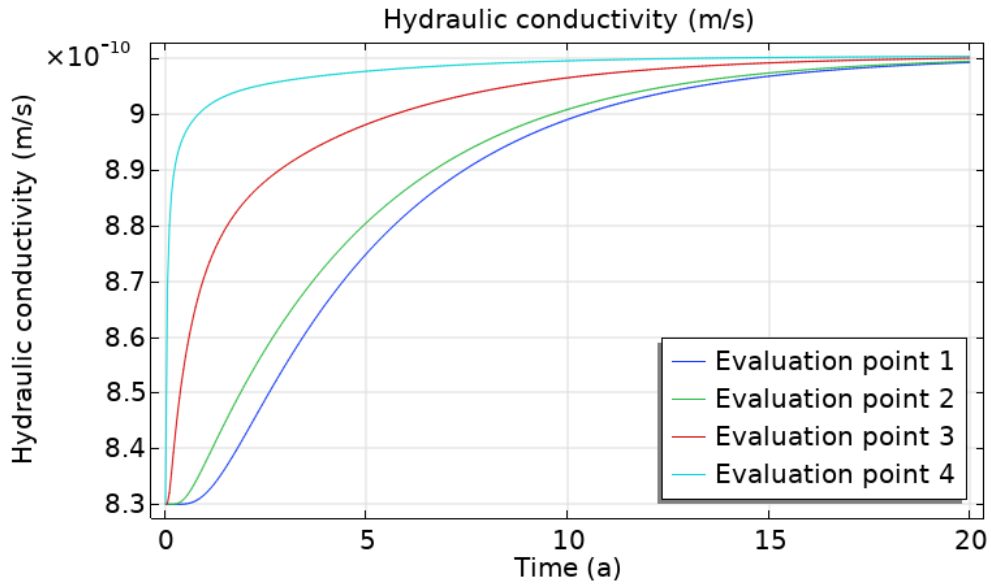
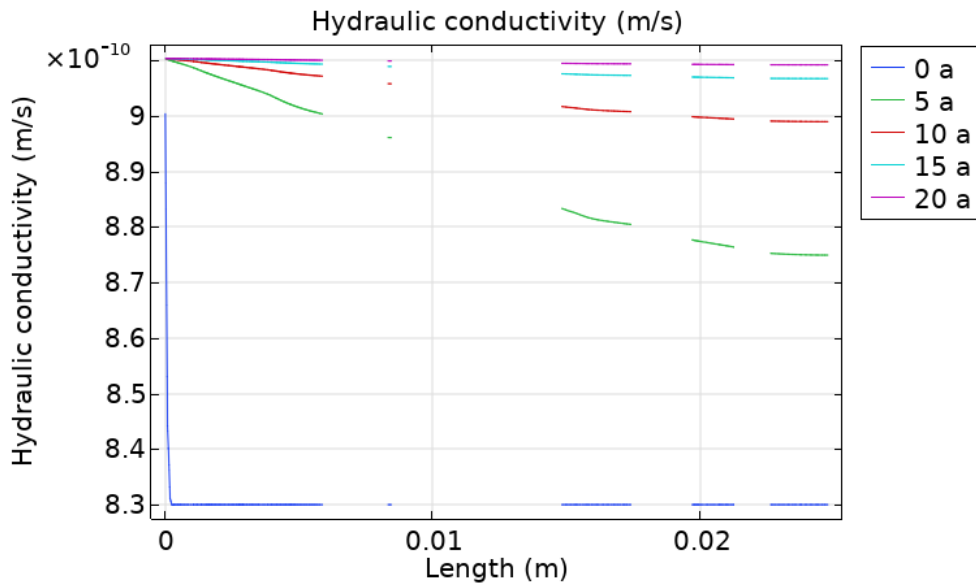*Figure 37: Variation of Hydraulic conductivity in time at four different points.*

Figure 38: Hydraulic conductivity values over the length of the domain at four different output times.

4.2 Three-dimensional Model

The three-dimensional model results are very similar to the ones obtained for the two-dimensional geometry and shown in the previous paragraph.

4.2.1 Steady-state Simulation

Figure 39 shows the hydraulic head distribution that is generated as a result of the stationary study. As previously, the values range from 6 meters to 5.9975, resulting in a hydraulic gradient of 0.01. This gradient, then, gives rise to the velocity field reported in Figure 40. The velocity lower range is smaller than the one of the previous study, possibly due to the presence of the contact points that alter the groundwater flow path.
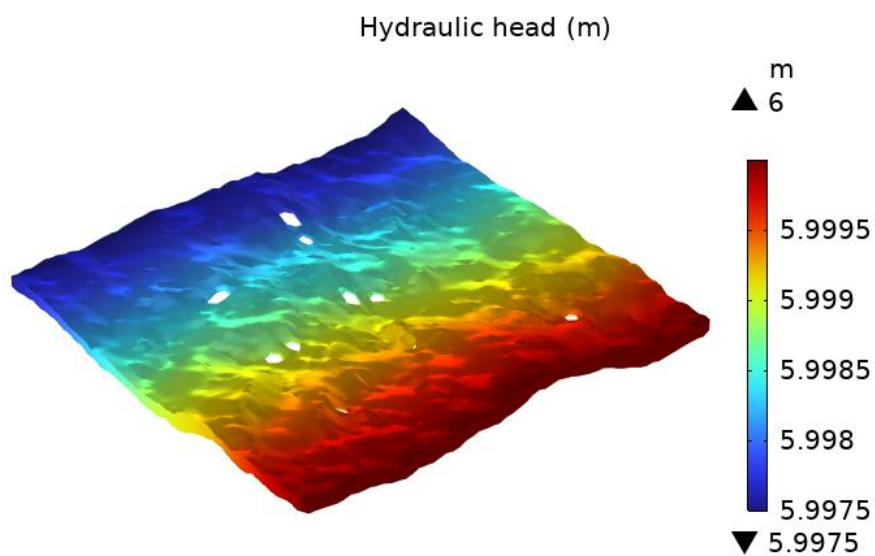

Figure 39: Steady-state results showing the hydraulic head in the three-dimensional domain.
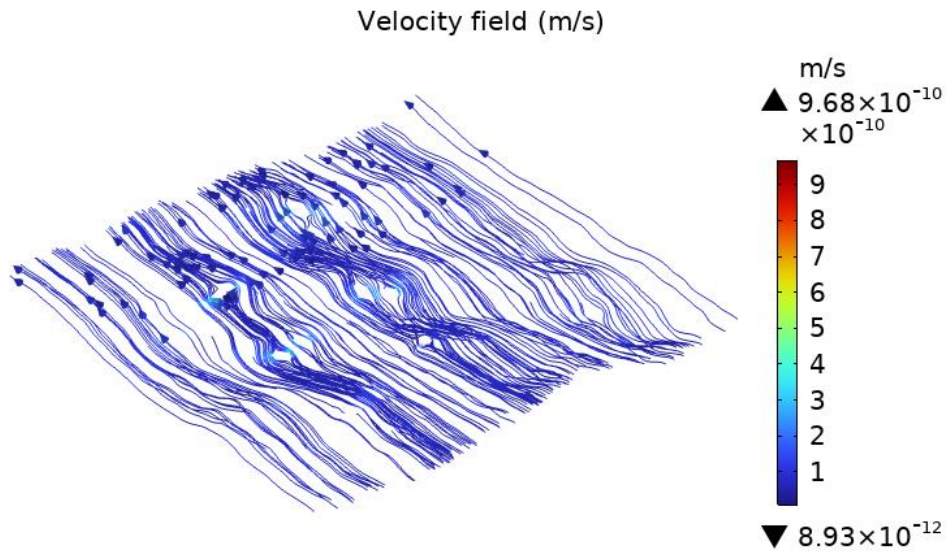
Velocity field (m/s)

Figure 40: Steady-state results showing the velocity field in the three-dimensional domain.

Figure 41, Figure 42, Figure 43, and Figure 44 present the values of the four chemical compounds in the domain at the end of the computation. The values are in accordance with what was estimated as the initial values in the porewater before the infiltrating solution starts to move inside the domain.
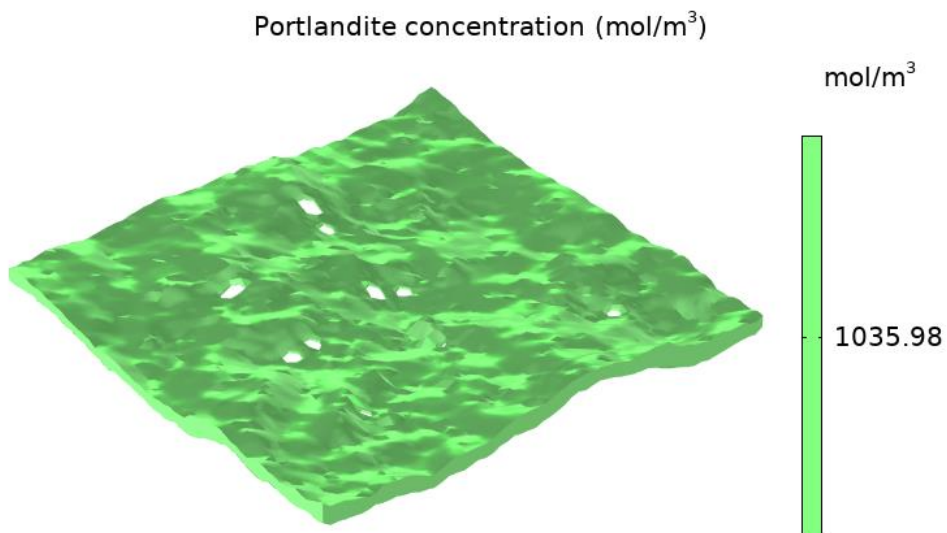
Portlandite concentration (mol/m³)

Figure 41: Steady-state simulation results showing Portlandite concentration.

Ca+2 concentration (mol/m³)
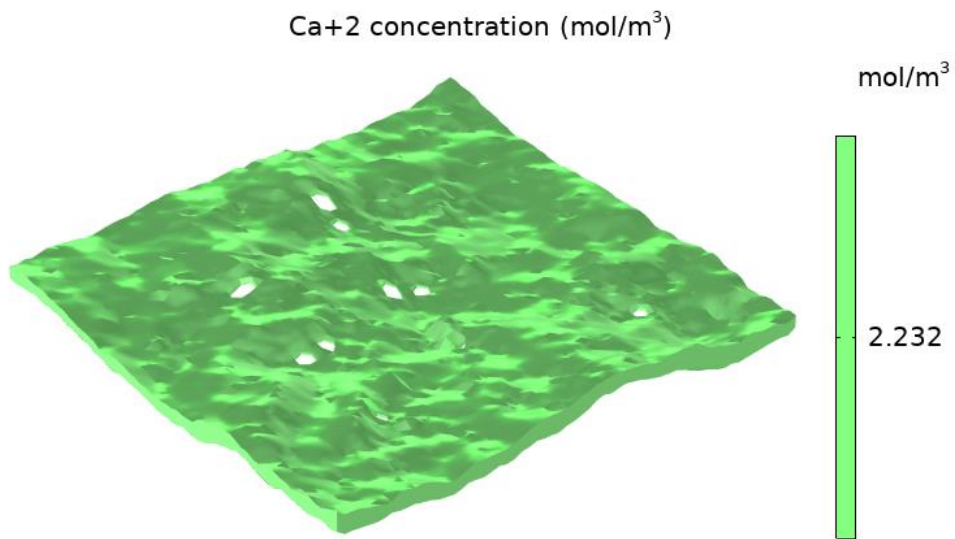
Figure 42: Steady-state simulation results showing calcium ions concentration.

H+ concentration (mol/m³)
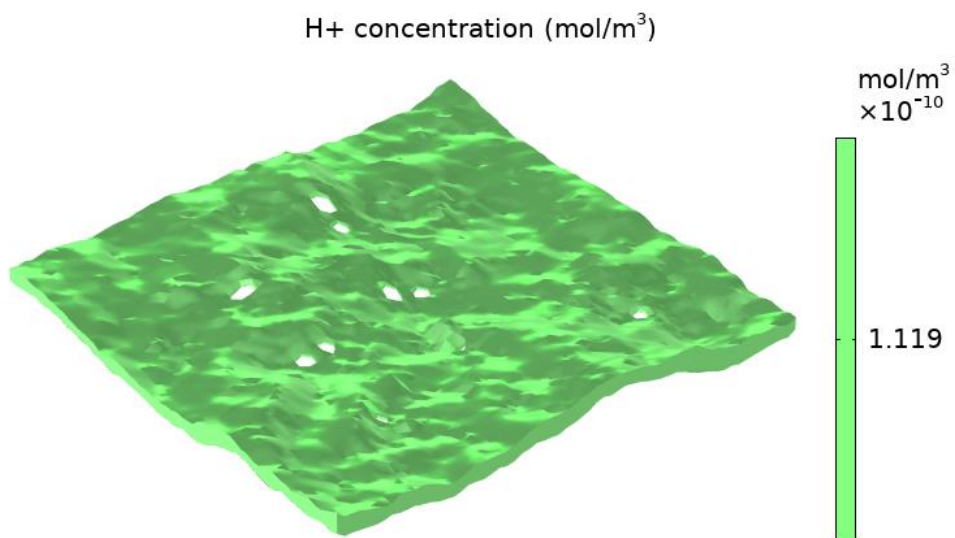
Figure 43: Steady-state simulation results showing hydrogen ions concentration.
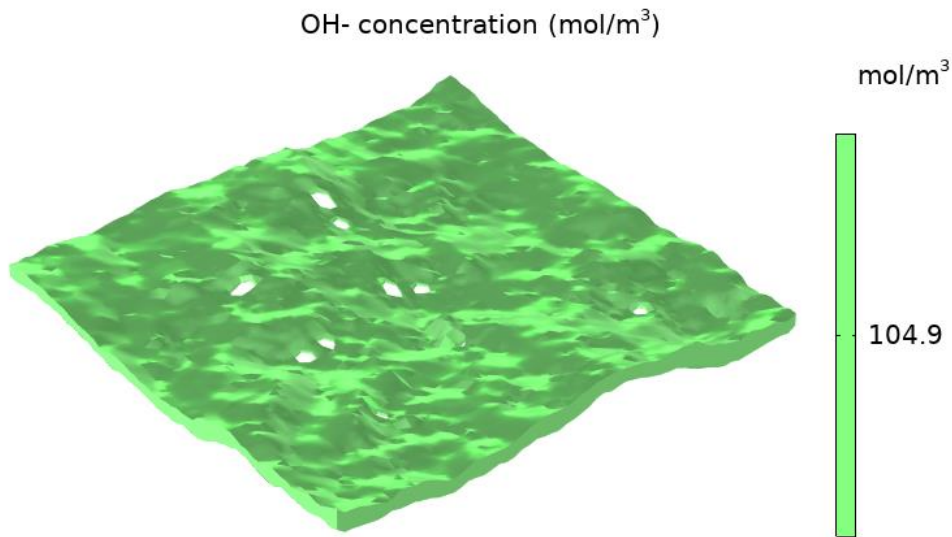
OH- concentration (mol/m^3)

Figure 44: Steady-state simulation results showing hydroxide ions concentration.

4.2.2 Time-dependent Simulation

After 20 years have passed, the results show that the concentration reached in the domain for the species varies spatially. Once again the left boundary where the infiltrating water inflows the domain reaches the estimated concentrations, whereas the rest of the domain assumes similar values but slightly higher. This can all be seen from Figure 45 to Figure 48.

Time=20 a   Portlandite concentration (mol/m³)

Figure 45: Transient simulation results after 20 years showing Portlandite concentration.

Time=20 a   Ca+2 concentration (mol/m³)

Figure 46: Transient simulation results after 20 years showing calcium ions concentration.
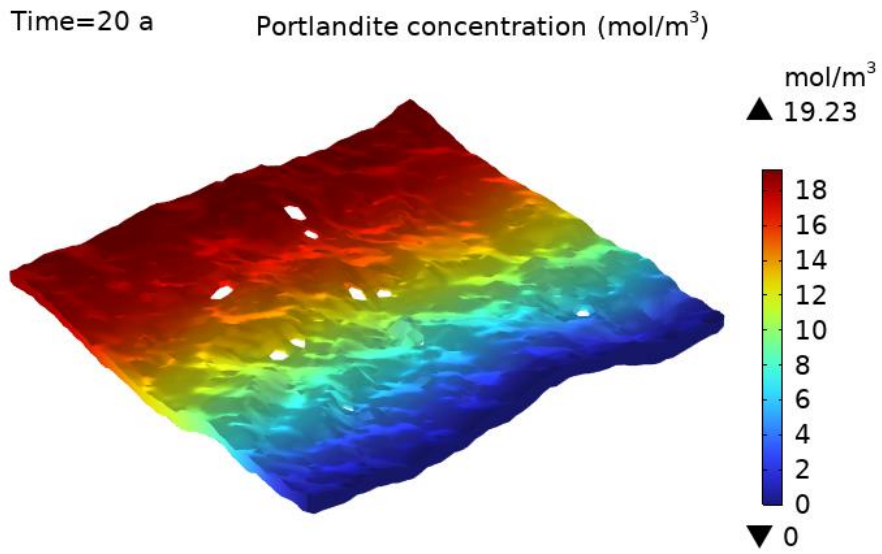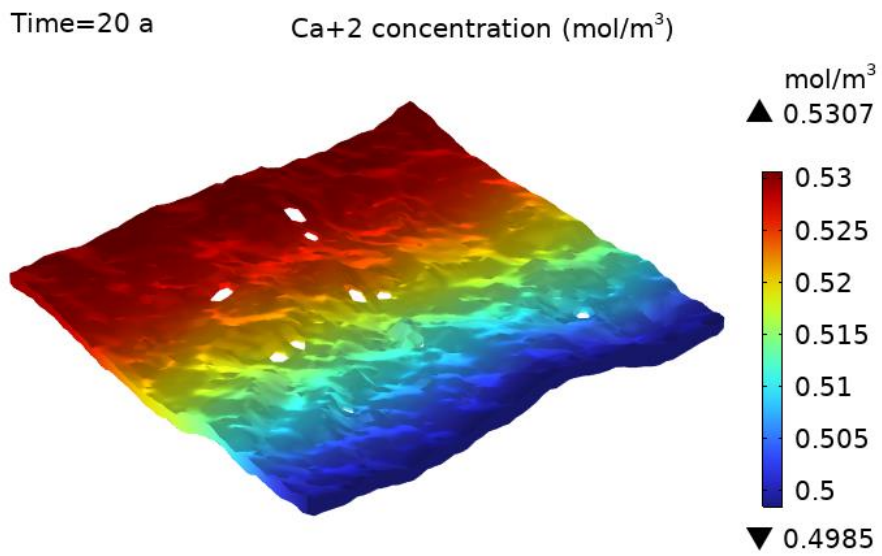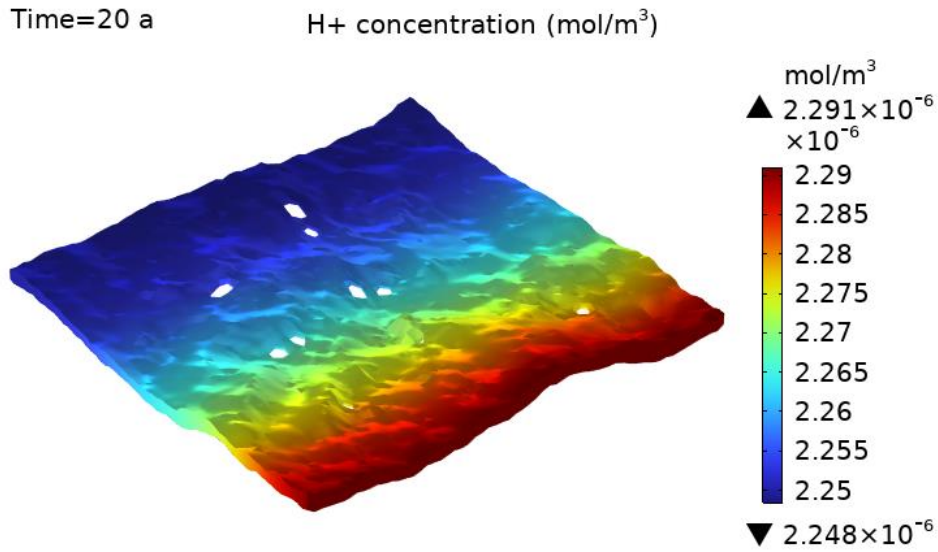
Figure 47: Transient simulation results after 20 years showing hydrogen ions concentration.
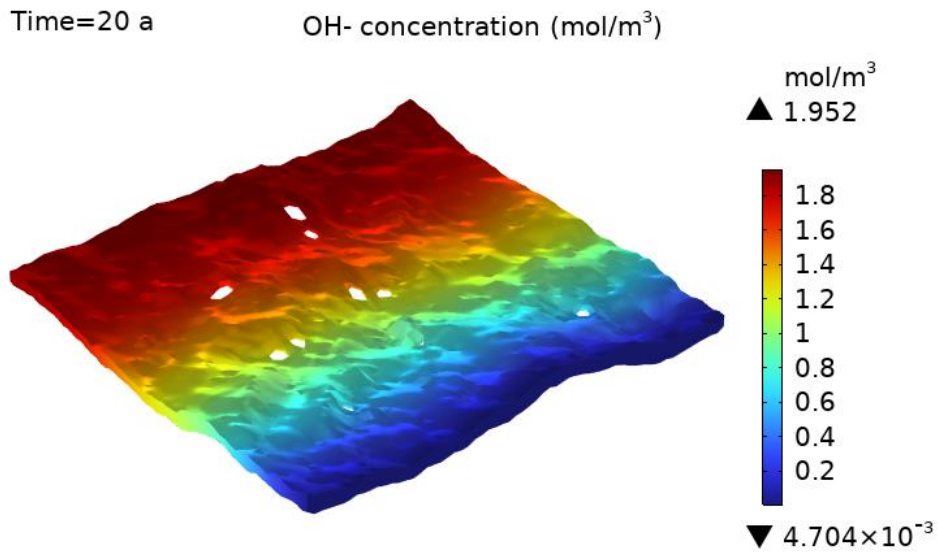
Figure 48: Transient simulation results after 20 years showing hydroxide ions concentration.

The plots shown from Figure 49 to Figure 52 assume a similar pattern as in the two-dimensional study, but in this case, the rate at which the final values are reached is slightly slower. The first point to reach the concentration of the inflowing groundwater is the one closer to the inlet boundary, while the outlet boundary is the last one to do so.

As for the spatially varying plots in Figure 53, Figure 54, Figure 55, and Figure 56, there is once again the presence of the initially pronounced gradient, that gets smoother over time. The first five years of the simulation are characterized by the strongest changes in concentration.
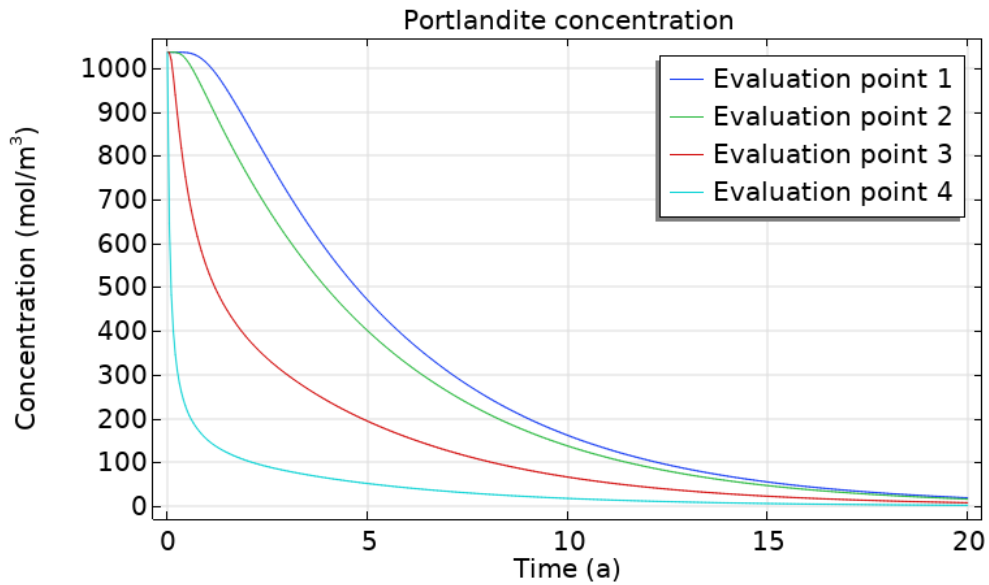

Figure 49: Evolution of the concentration in time at four different points for Portlandite.
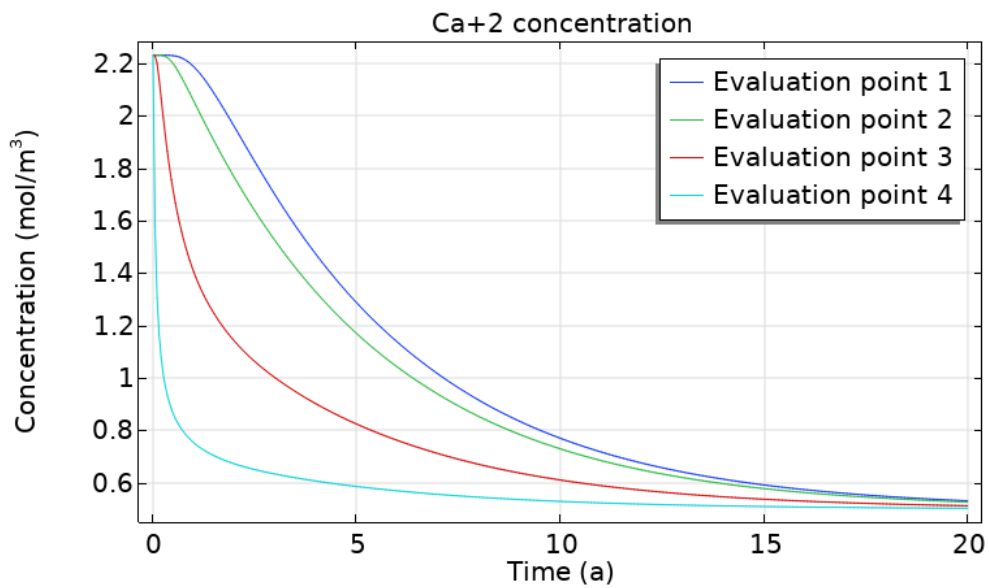
Figure 50: Evolution of the concentration in time at four different points for calcium ions.

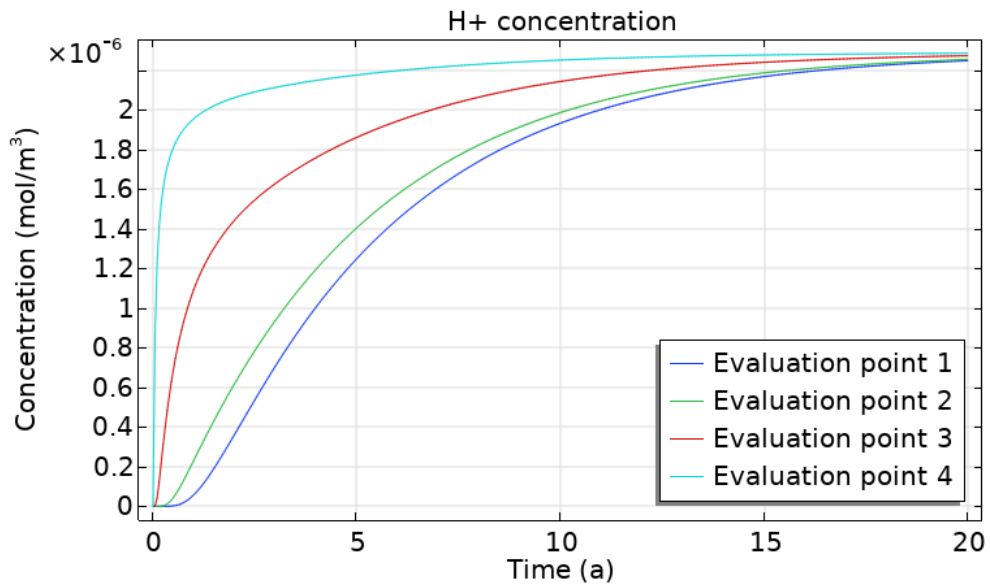*Figure 51: Evolution of the concentration in time at four different points for hydrogen ions.*
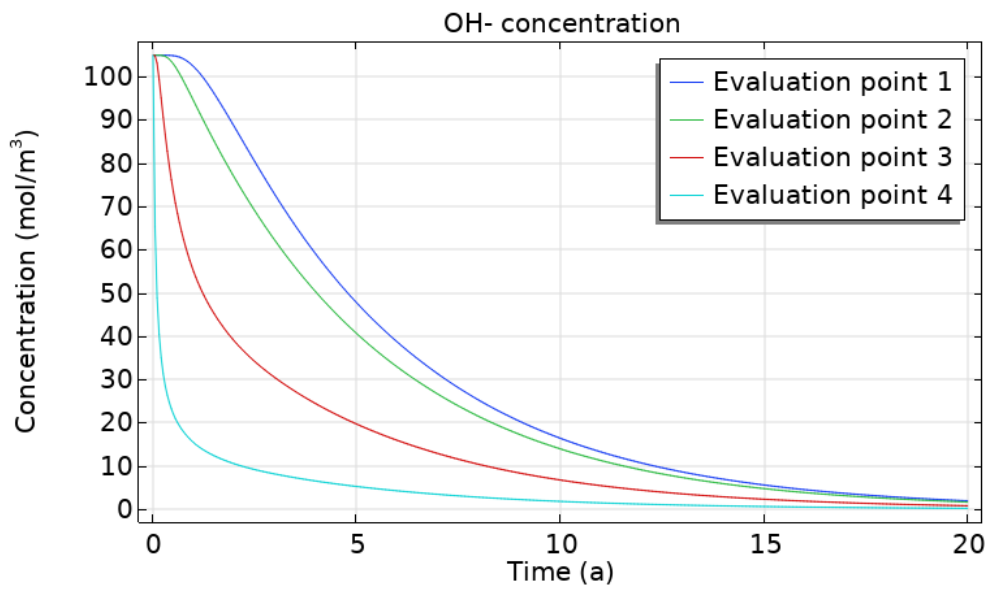
Figure 52: Evolution of the concentration in time at four different points for hydroxide ions.
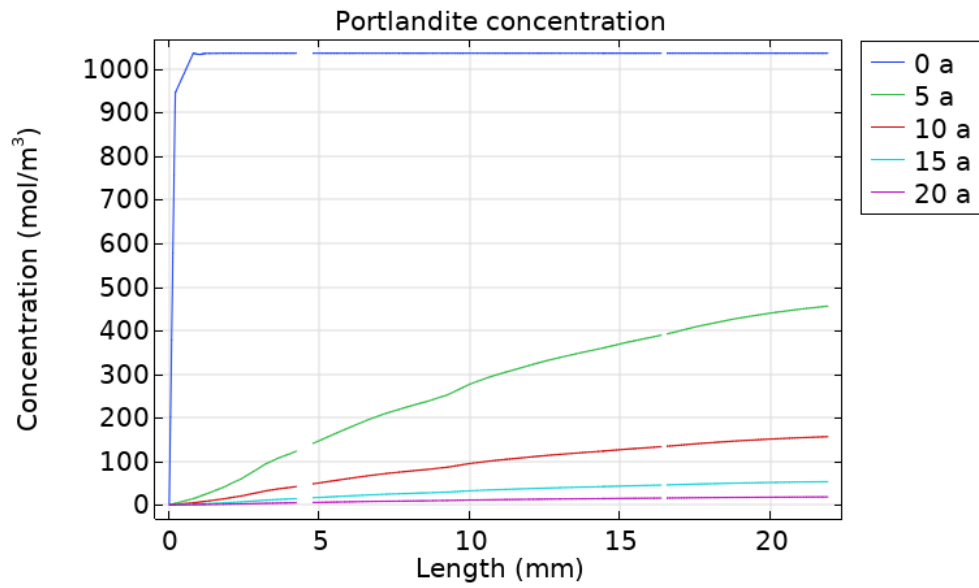
Figure 53: Concentration values over the length of the domain at different output times for Portlandite.
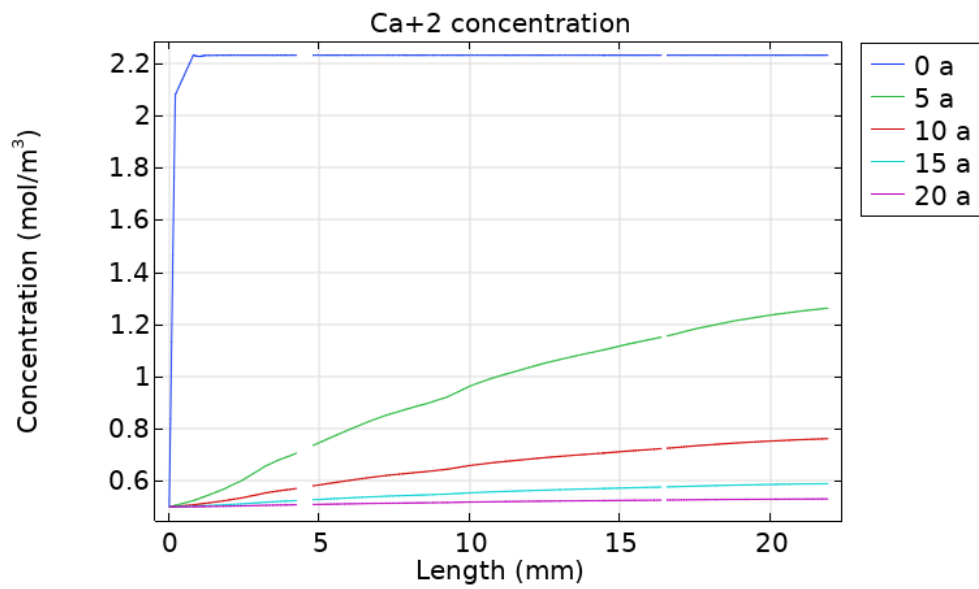
Figure 54: Concentration values over the length of the domain at different output times for calcium ions.
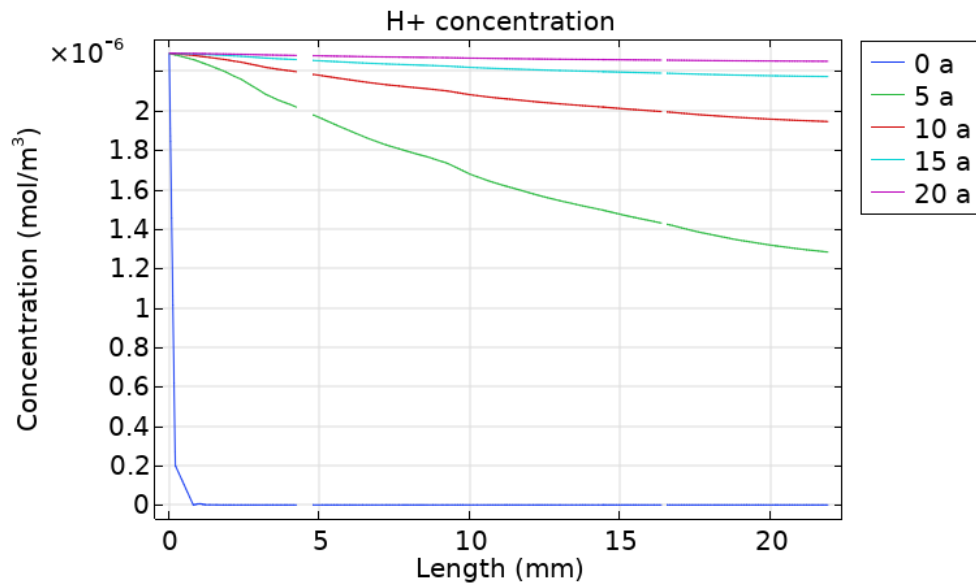
Figure 55: Concentration values over the length of the domain at different output times for hydrogen ions.
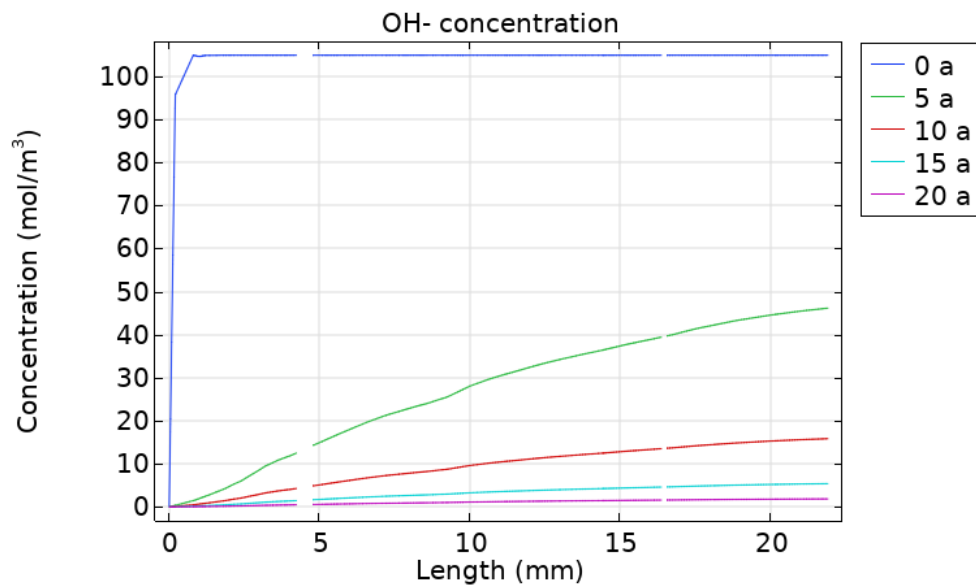
Figure 56: Concentration values over the length of the domain at different output times for hydroxide ions.

The pH meets the values indicated in Paragraph 2.2.1.2, for both the porewater and the infiltrating groundwater, as shown in Figure 57 and Figure 58. The plots in Figure 59 show a strong variation in pH for all the evaluating points, especially in the first five years. The dip in Figure 60 is caused by a fluctuation in the hydrogen ions concentration value, from which the pH was calculated.
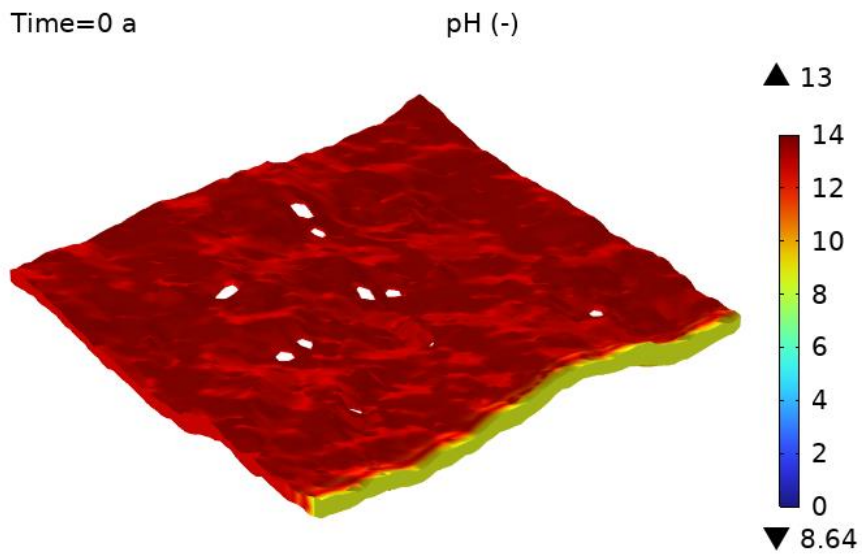
Figure 57: pH values in the whole domain at time 0.
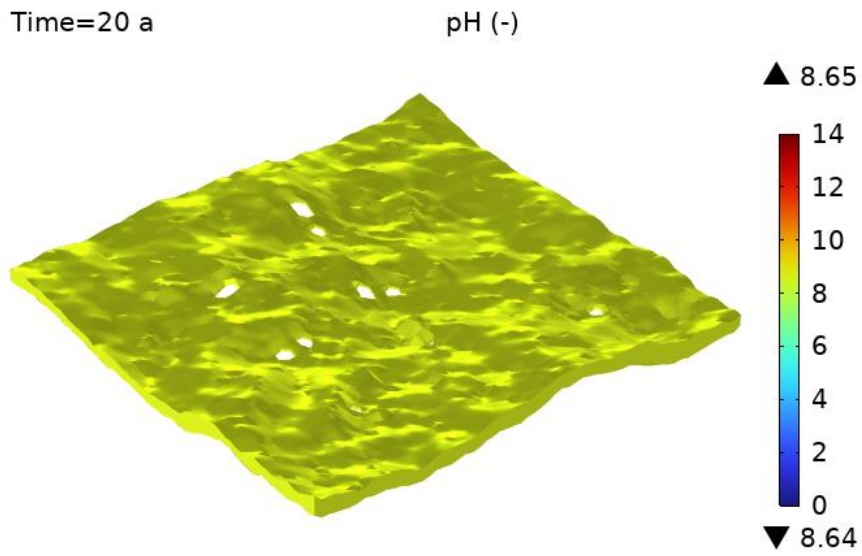
Figure 58: pH values in the whole domain after 20 years.
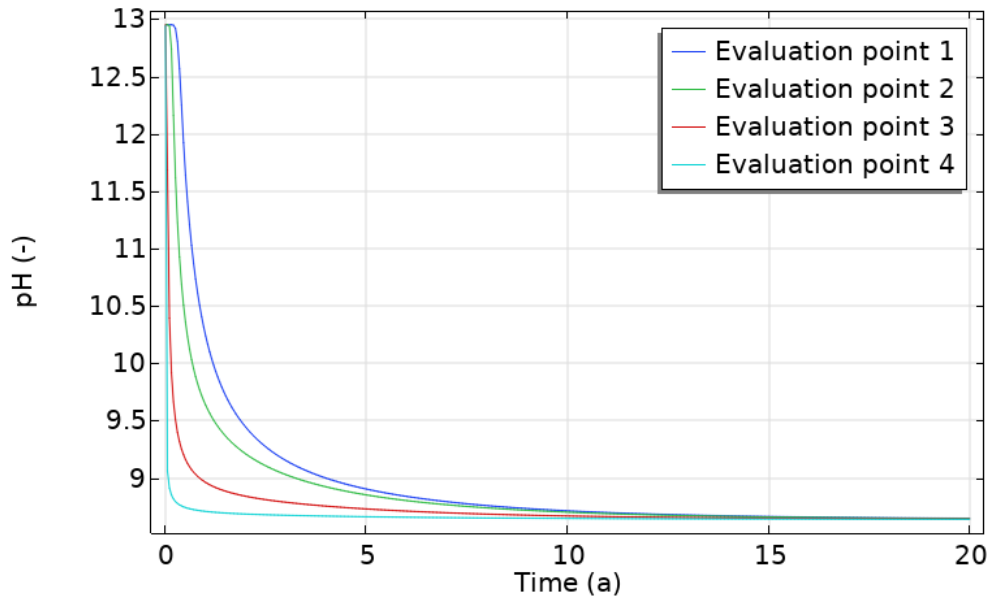
Figure 59: pH variation in time at four different points in the domain.
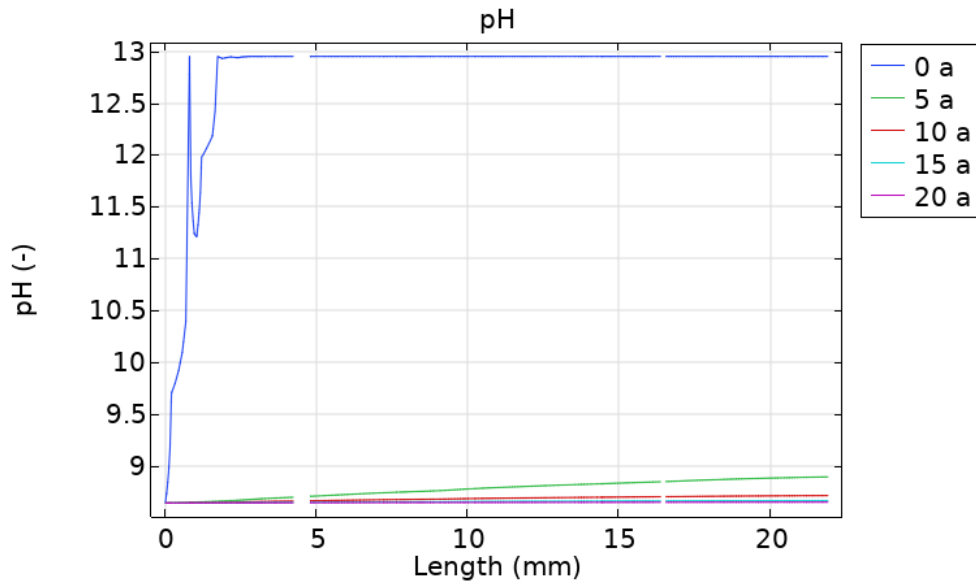
Figure 60: pH values over the length of the domain at different output times.

Ultimately, the new values of porosity and hydraulic conductivity were calculated. The initial values across the domain are shown in Figure 61 and Figure 63. The range of values for the properties after 20 years are shown in Figure 62 and Figure 64, they match the one of the two-dimensional case. However, by looking at the plots in Figure 65, Figure 66, Figure 67, and Figure 68, the speed at which these values are reached is slightly slower.

The reason for that is to be found in the lower velocity values and, therefore, in the higher times required for the displacement front to move inside of the domain.
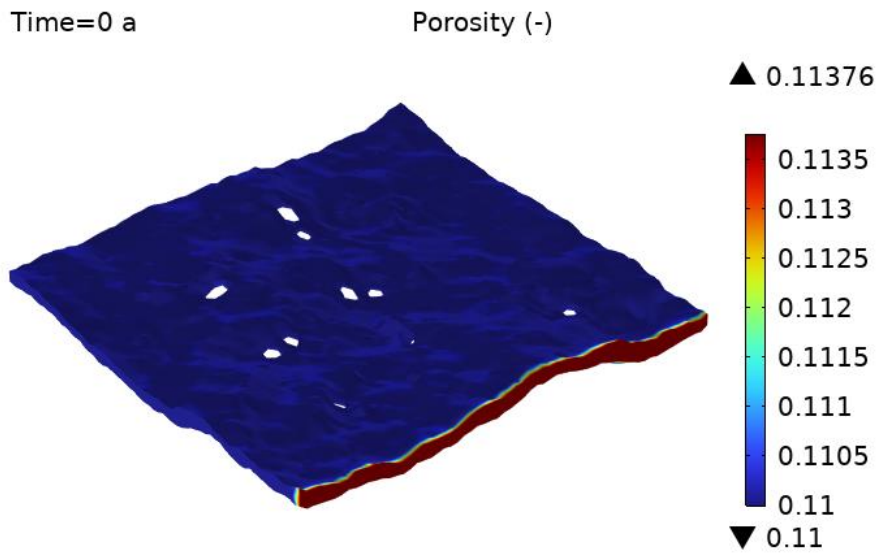
Figure 61: Porosity values at the beginning of the simulation.
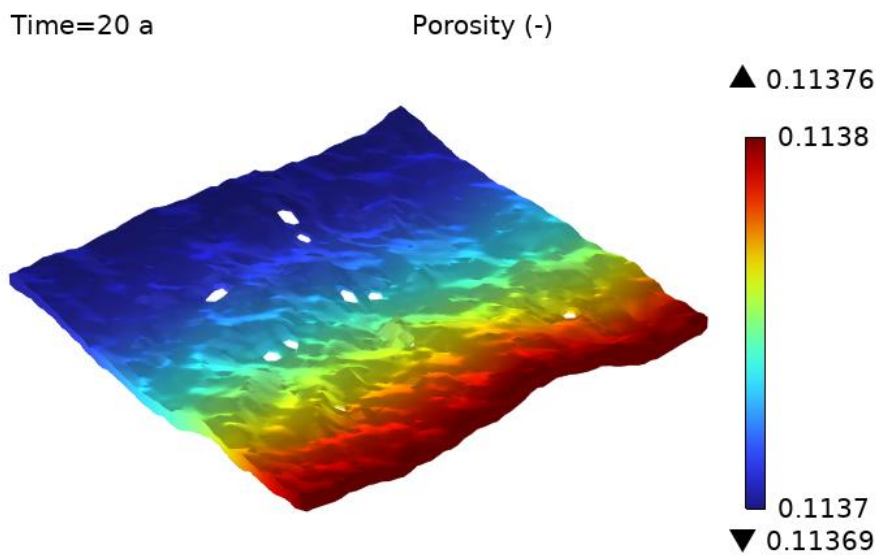
Figure 62: Porosity values after 20 years.
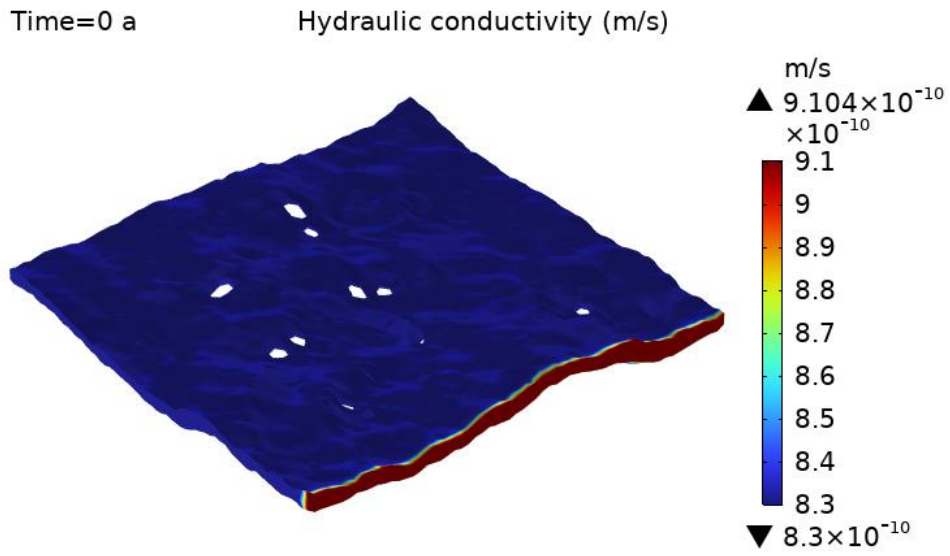
Figure 63: Hydraulic conductivity values at the beginning of the simulation.
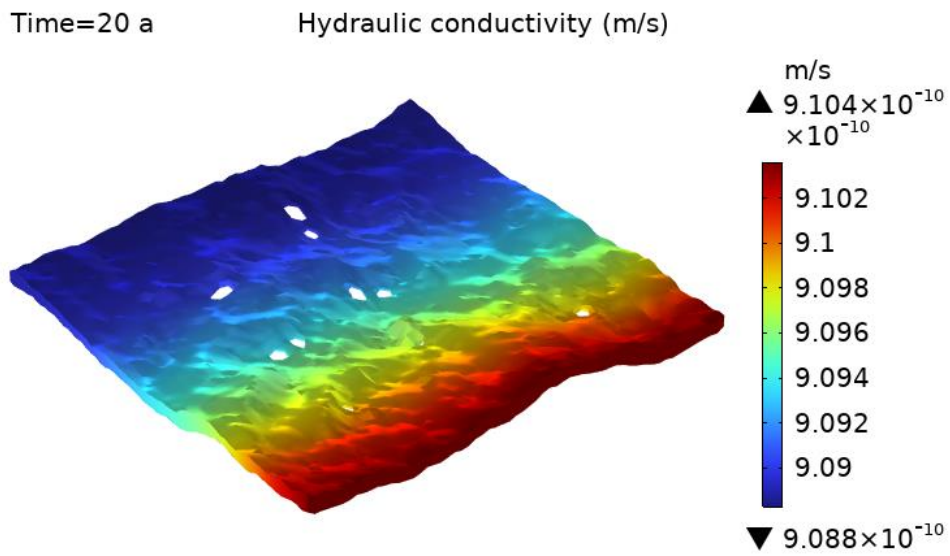
Figure 64: Hydraulic conductivity values after 20 years.
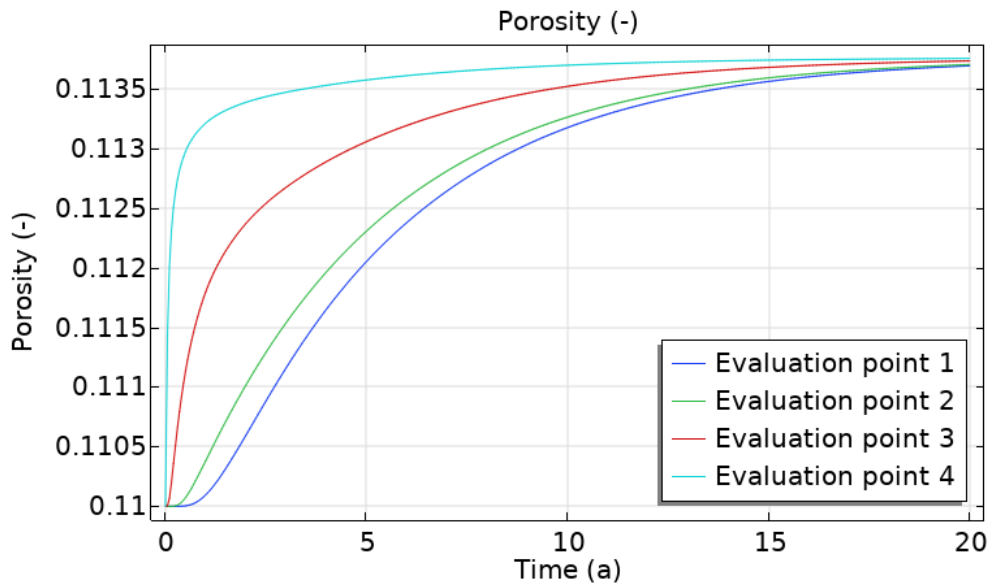
Figure 65: Variation of porosity in time at four different points.
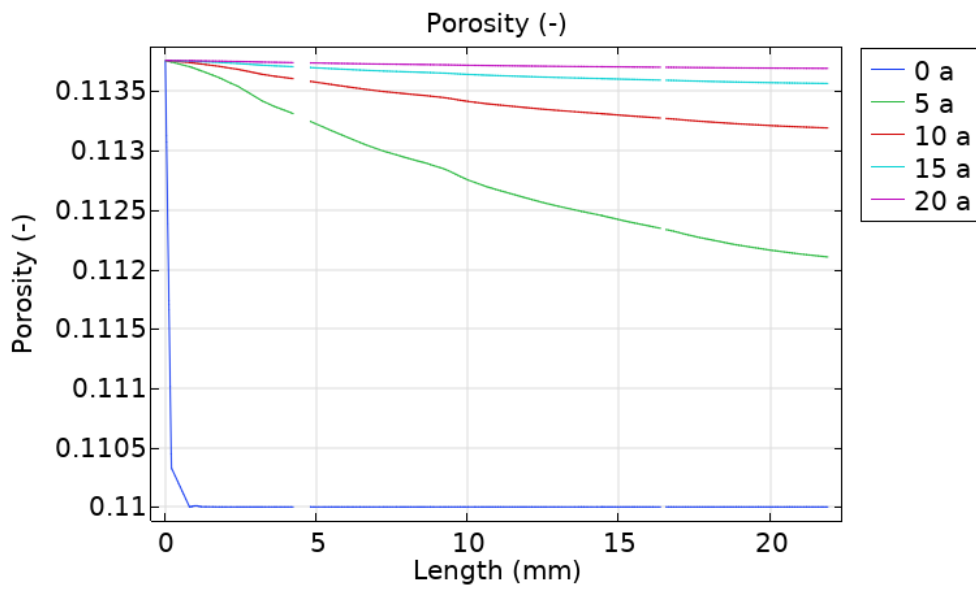
Figure 66: Porosity values over the length of the domain at four different output times.
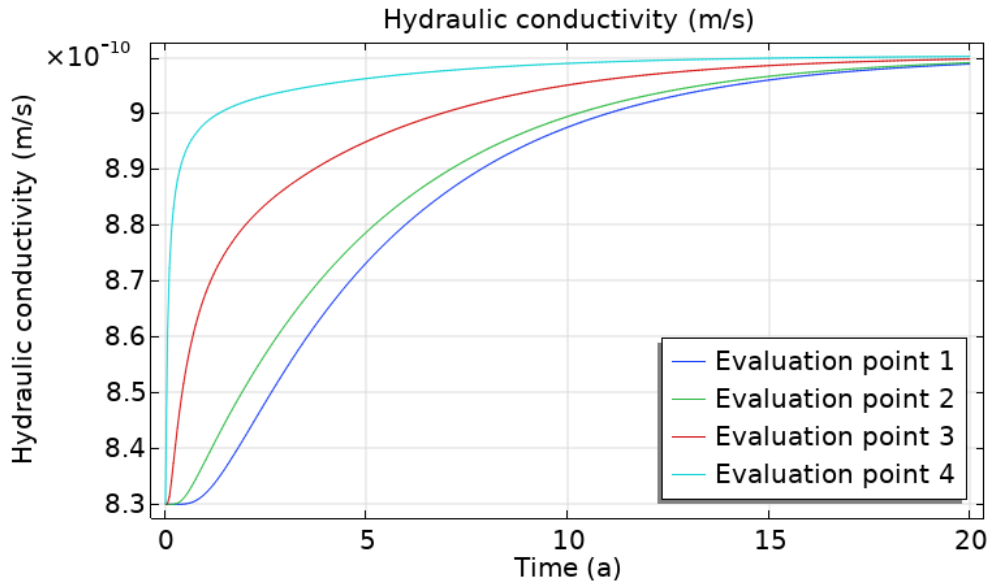
Figure 67: Variation of hydraulic conductivity in time at four different points.
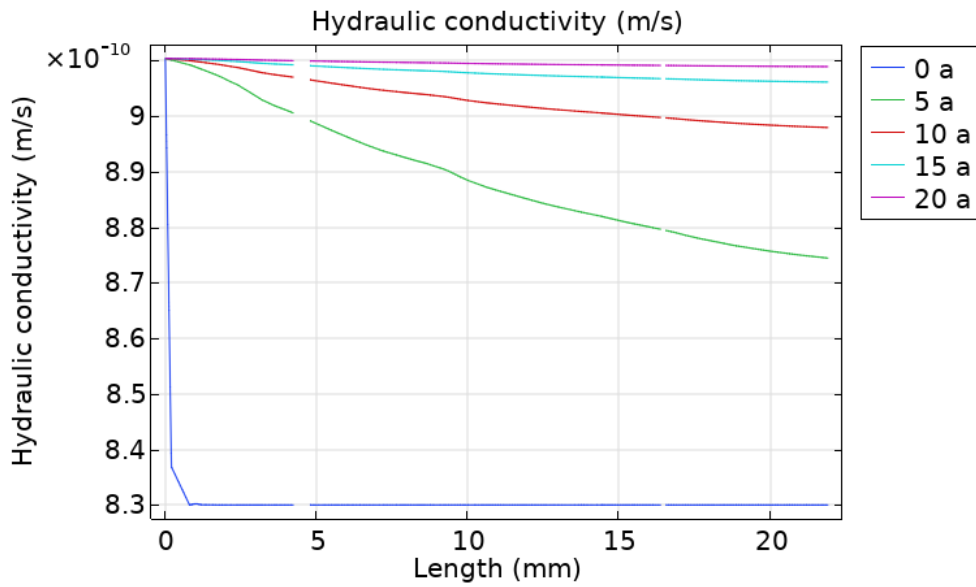
Figure 68: Hydraulic conductivity values over the length of the domain at four different output times.

5   Discussion

The results confirmed that after the system has reached equilibrium and the portlandite present in the cement grout has been dissolved by the porewater, the inflow of an infiltrating groundwater solution not containing calcium hydroxide will gradually mobilize the mineral. As the portlandite is carried out of the domain over time, new voids are formed in the porous matrix. Because of this, the value of hydraulic properties such as porosity and hydraulic conductivity will increase over time, allowing more groundwater to flow through the domain., as stated by Luna, Arcos, and Duro (2006).

Gayscone (2002) highlights how the presence of unreacted portlandite in the grout porewater maintains the pH at around 12.5, and that its removal from the environment will cause the acidification of the solution. Indeed, the porewater's initial pH was 12.951 due to the low concentration of hydrogen ions. Both the two-dimensional and three-dimensional models had the same value of pH at the beginning of the time-dependent simulation. As the infiltrating solution was allowed to flow through the domain, removing the portlandite from the saturated matrix, the pH decreased to a range of values of 8.65÷8.64 in both the two-dimensional and three-dimensional cases. This range matched the pH of the infiltrating groundwater, which was 8.64.

After 20 years, the concentration of the chemical species in the domain is consistent with the molarities computed using the software PHREEQC. The left boundary, the one where the Concentration BC was applied, has the expected values and moving towards the outflow boundary, the concentration increases. As the two-dimensional model had a higher velocity field, the molarities at the outflowing boundary are lower compared to the

ones computed at the same point for the three-dimensional model. However, the reason for that could be found in the presence of contact points between the upper and lower surfaces, which can hinder the groundwater flow.

The biggest variations in the concentration of the species took place in the first 10 years of the simulation for both geometries, whereas for the pH the change was faster, as it decreased significantly in the first 5 years.

While these changes happened at different paces for the two simulations, the final results concerning the cement grout degradation are the same. In fact, both models have shown an increase in the magnitude of porosity of 3.45%, while the value of hydraulic conductivity increased by 9.64%. This fact is of crucial importance, since as Liu et al. (2018) state the grout is needed to prevent the groundwater from reaching foundations and eroding them. So in the case of this study, which analyses changes in hydraulic properties in the grout located under dam foundations, the risk of structural instabilities and failure can increase as the cement grout becomes more permeable to water.

The set-up of two steady-state simulations, one for each geometry, which results represented the considered systems at equilibrium before the inflow of a new solution took place, allowed to determine the initial values for the transient studies. This additional step was added because COMSOL (no date) states that by doing so, the initial values will be consistent with the solution and therefore the convergence of the models will be improved.

Various limitations have to be taken into account in this thesis. The first one is that the only mineral evaluated is portlandite. Moreover, only its dissolution has been considered, while other processes such as adsorption were neglected. Other minerals present in the cement grout can dissolve, causing the precipitation of secondary crystalline species. This leads to an iterative process that can affect the final variations in porosity and hydraulic conductivity.

A single cement composition has been utilized, but it's important to remember that this can vary largely from one manufacturer to another based on the raw materials composition. Therefore, as the final outcomes wouldn't be too far from what this analysis has found, the variations in concentrations, pH, and matrix properties would probably have slightly different final values.

5 - DISCUSSION

The porosity and hydraulic conductivity variations have been obtained from the final results, while the models run without changes in properties. Future research should focus on creating an iterative model which can compute the porosity and hydraulic conductivity at each time step so that the velocity and the final mineral concentration would both be affected by the iterative changes.

Future studies should focus on including more if not all mineral phases present in the cement grout, as well as other chemical processes such as adsorption and mineral precipitation. By doing so, it would be possible to assess whether the porosity and hydraulic conductivity increase as it was found, more, or even less.

The results of this study could be applied to determine the amount of groundwater reaching the foundations of the overlying dam to properly assess their erosion, thereby studying the risks of structural instabilities that can arise.

6 Conclusions

The purpose of this thesis was to assess the variation in porosity and hydraulic conductivity in the cement grout injected in a rock fracture located under a dam. In the long term, the grout degradation would lead to the risk of foundation erosion and consequently structural failure.

Two models have been run using the software COMSOL Multiphysics®, a two-dimensional one representing a fracture of infinite extent and a three-dimensional one, built by coupling the fluid flow component to the transport one. Steady-state simulations were computed to improve the convergence of the two transient models.

The results show that after 20 years, there is a significant decrease in portlandite concentration in both geometries. The biggest variation occurred in the two-dimensional model due to the overall higher velocity values, which the absence of contact points between the upper and lower surfaces of the fracture may cause. The variation in porosity and hydraulic conductivity was computed in post-processing. The pH values decreased in the two-dimensional and three-dimensional cases from 12.951 to 8.65÷8.64. The changes in chemical species concentration mainly occurred in the first ten years, while the pH decreased to values lower than 9 in the first five years. Although the slight differences in final molarities of the two models, the increase in porosity and hydraulic conductivity had the same magnitude, with the first increasing by 3.45% and the latter by 9.64%.

6 - CONCLUSIONS

The study is however subject to multiple limitations. The most important one is that portlandite is the only mineral included in the simulations, while other phases were left out. Considering that precipitation and sorption are also neglected, many possible interactions between different minerals that could be more representative of real scenarios are ignored. Furthermore, the absence of coupling between portlandite concentration decrease and hydraulic properties changes represents another limitation, given that these variations influence one another. The porewater chemical makeup was based on OPC composition. Even though the latter performance is good, in areas associated with stronger portlandite depletion other cement types could represent a more valid alternative. These finding can be useful in determining the amount of groundwater that is able to pass through the grouted fracture and reach the dam foundations, helping therefore to determine the risk of structural instabilities and failure in the future.

Future studies should focus on including more, if not all, mineral phases as well as other chemical processes such as adsorption and mineral precipitation, to determine whether porosity and hydraulic conductivity alteration will vary compared to the findings of this thesis. In addition to reproduce more realistically the degrading process, the models should implement a coupling between groundwater flow, reactive transport, and porosity and hydraulic conductivity variations. Such an approach would allow the simulation to be iterative, making the varying properties influence the flow and vice versa. This solution would yield more accurate results. Given that no clear conclusion could be drawn about the effects of different infiltrating groundwater solutions, studies could focus on understanding this aspect better.

7   References

Aïtcin, P.-C. (2016) '3 - Portland Cement', in Aïtcin, P.-C., Flatt, R.J. (ed.) *Science and Technology of Concrete Admixtures*. Cambridge, UK: Woodhead Publishing, An Imprint Of Elsevier, pp. 27 – 51.

COMSOL (2016) *The Finite Element Method*. Available at: https://www.comsol.it/multiphysics/finite-element-method (Accessed 4 June 2024).

COMSOL (2018) *CDF Module User's Guide.* Available at: https://www.google.com/url?sa=t&source=web&rct=j&opi=89978449&url=https://doc.comsol.com/5.4/doc/com.comsol.help.cfd/CFDModuleUsersGuide.pdf&ved=2ahUKEwil57K398aGAxWXJBAIHTeLBqkQFnoECBEQAQ&usg=AOvVaw0xopu0eiXjKSq7vF1UD7Tj

COMSOL (no date) *How to Build a Mesh in COMSOL Multiphysics®.* Available at: https://www.comsol.com/video-training/getting-started/building-the-mesh-for-a-model-geometry-in-comsol-multiphysics#:~:text=Mesh%20%2F%20Basics%20of%20Meshing&text=The%20mesh%20used%20for%20a,of%20elements%20in%20the%20geometry (Accessed 9 October 2024).

COMSOL (no date) *Solving Transient Models That Have Inconsistent Initial Values.* Available at: https://www.comsol.com/support/learning-center/article/Solving-Transient-Models-That-Have-Inconsistent-Initial-Values-46461 (Accessed 9 October 2024).

da Silva, M.T.Q.S., Do Rocio Cardoso, M., Veronese, C.M.P. and Mazer, W. (2022) 'Tortuosity: A Brief review', *Materials Today: Proceedings*, 58, pp. 1344 – 1349. Available at: https://doi.org/10.1016/j.matpr.2022.02.228

7 - REFERENCES

Deng, S., Wang, X., Yu, J., Zhang, Y., Liu, Z., Zhu, Y. (2018) 'Simulation of Grouting Processes in Rock Masses Under a Dam Foundation Characterized by a 3D Fracture Network', *Rock Mechanics and Rock Engineering*, 51, pp. 1801 – 1822. Available at: https://doi.org/10.1007/s00603-018-1436-y

Fernandez-Gutierrez, J.D., Sanches Rodriguez, S., Gonzalo-Orden, H., and Perez-Acebo, H. (2021) 'Analysis of rock mass classifications for safer infrastructures', *Transport Research Procedia*, 58, pp. 606 – 613. Available at: https://doi.org/10.1016/j.trpro.2021.11.080

Fetter, C.W. and Kreamer, D. (2022) *Applied Hydrogeology*. Fifth Edition. Long Grove, IL: Waveland Press, Inc.

Gascoyne, M. (2002). *Influence of grout and cement on groundwater composition*. Working report No. 2002-07. Pinawa, Manitoba, Canada: Gascoyne GeoProjects Inc. Available at:
https://www.researchgate.net/publication/267250725_Working_Influence_of_grout_and_cement_on_groundwater_composition

Gothäll, H. (2022) *How to Inspect Your Mesh in COMSOL Multiphysics®.* Available at: https://www.comsol.it/blogs/how-to-inspect-your-mesh-in-comsol-multiphysics (Accessed 9 October 2024).

Idiart, A. and Shafei, B. (2019). *Modelling of concrete degradation – Hydro-chemical processes: Report for the safety evaluation SE-SFL*. Report No. R-19-11. Solna, Sweden: Svensk Kärnbränslehantering AB. Available at: https://www.skb.com/publication/2493299

Jazayeri, A., Werner, A.D. (2019) 'Boundary Condition Nomenclature Confusion in Groundwater Flow Modeling', *Groundwater*, 57(5), pp. 664 – 668. Available at: https://doi.org/10.1111/gwat.12893

7 - REFERENCES

Liu, J., Li, Y., Zhang, G., Liu, Y. (2019) 'Effects of cementitious grout components on rheological properties', *Construction and Building Materials*, 227, pp.116654 – 116654. Available at: https://doi.org/10.1016/j.conbuildmat.2019.08.035

Liu, Q., Lei, G., Peng, X., Lu, C., and Wei, L. (2018) 'Rheological Characteristics of Cement Grout and its Effects on Mechanical Properties of a Rock Fracture', *Rock Mechanics and Rock Engineering*, 51, pp. 613 – 625. Available at: https://doi.org/10.1007/s13146-020-00619-z

Lothenbach, B., Kulik, D.A., Matschei, T., Balonis, M., Baquerizo, L., Dilnesa, B., Miron, G.D., Myers, R.J. (2019) 'CEMDATA18: A chemical thermodynamic database for hydrated Portland cements and alkali-activated materials', *Cement and Concrete Reasearch*, 115, pp. 472 – 506. Available at: https://doi.org/10.1016/j.cemconres.2018.04.018

Luna, M., Arcos, D., and Duro, L. (2006) *Effects of grouting, shotcreting and concrete leachates on backfill geochemistry*. Report No. R-06-107. Enviros, Spain: Svensk Kärnbränslehantering AB. Available at: https://www.skb.com/publication/1335868

Marchon, D. and Flatt, R.J. (2016) '8 - Mechanisms of cement hydration', in Aïtcin, P.-C., Flatt, R.J. (ed.) *Science and Technology of Concrete Admixtures*. Cambridge, UK: Woodhead Publishing, An Imprint Of Elsevier, pp. 129 – 145.

Sethi, R. and Di Molfetta, A. (2019) *Groundwater Engineering: A Technical Approach to Hydrogeology, Contaminant Transport and Groundwater Remediation*. Cham, Switzerland: Springer.

Sha, F., Lin, C., Li, Z., and Liu, R. (2019) 'Reinforcement simulation of water-rich and broken rock with Portland cement-based grout', *Construction and Building Materials*, 221, pp. 292 – 300. Available at: https://doi.org/10.1016/j.conbuildmat.2019.06.094

7 - REFERENCES

78

Zou, L., Jing, L. and Cvetkovic, V. (2017) 'Shear-enhanced nonlinear flow in rough-walled rock fractures', *International Journal of Rock Mechanics and Mining Sciences*, 97, pp. 33 – 45. Available at: https://doi.org/10.1016/j.ijrmms.2017.06.001